U.S. DEPARTMENT OF COMMERCE
NATIONAL OCEANIC AND ATMOSPHERIC ADMINISTRATION
OCEAN PRODUCTS CENTER

TECHNICAL NOTE

DEVELOPMENT OF A SINGLE "ALL-WEATHER" NEURAL NETWORK ALGORITHM FOR ESTIMATING OCEAN SURFACE WINDS FROM THE SPECIAL SENSOR MICROWAVE IMAGER

V. M. KRASNOPOLSKY, L. C. BREAKER, AND W. H. GEMMILL

NATIONAL METEOROLOGICAL CENTER
WASHINGTON, D.C.
JUNE 1994

---

*OPC Contribution No. 94

OPC CONTRIBUTIONS

No. 1. Burroughs, L. D., 1987: Development of Forecast Guidance for Santa Ana Conditions. National Weather Digest, Vol. 12 No. 1, 7pp.

No. 2. Richardson, W. S., D. J. Schwab, Y. Y. Chao, and D. M. Wright, 1986: Lake Erie Wave Height Forecasts Generated by Empirical and Dynamical Methods -- Comparison and Verification. Technical Note, 23pp.

No. 3. Auer, S. J., 1986: Determination of Errors in LFM Forecasts Surface Lows Over the Northwest Atlantic Ocean. Technical Note/NMC Office Note No. 313, 17pp.

No. 4. Rao, D. B., S. D. Steenrod, and B. V. Sanchez, 1987: A Method of Calculating the Total Flow from A Given Sea Surface Topography. NASA Technical Memorandum 87799., 19pp.

No. 5. Feit, D. M., 1986: Compendium of Marine Meteorological and Oceanographic Products of the Ocean Products Center. NOAA Technical Memorandum NWS NMC 68, 93pp.

No. 6. Auer, S. J., 1986: A Comparison of the LFM, Spectral, and ECMWF Numerical Model Forecasts of Deepening Oceanic Cyclones During One Cool Season. Technical Note/NMC Office Note No. 312, 20pp.

No. 7. Burroughs, L. D., 1987: Development of Open Fog Forecasting Regions. Technical Note/NMC Office Note. No. 323., 36pp.

No. 8. Yu, T. W., 1987: A Technique of Deducing Wind Direction from Satellite Measurements of Wind Speed. Monthly Weather Review, 115, 1929-1939.

No. 9. Auer, S. J., 1987: Five-Year Climatological Survey of the Gulf Stream System and Its Associated Rings. Journal of Geophysical Research, 92, 11,709-11,726.

No. 10. Chao, Y. Y., 1987: Forecasting Wave Conditions Affected by Currents and Bottom Topography. Technical Note, 11pp.

No. 11. Esteva, D. C., 1987: The Editing and Averaging of Altimeter Wave and Wind Data. Technical Note, 4pp.

No. 12. Feit, D. M., 1987: Forecasting Superstructure Icing for Alaskan Waters. National Weather Digest, 12, 5-10.

No. 13. Sanchez, B. V., D. B. Rao, S. D. Steenrod, 1987: Tidal Estimation in the Atlantic and Indian Oceans. Marine Geodesy, 10, 309-350.

No. 14. Gemmill, W.H., T.W. Yu, and D.M. Feit 1988: Performance of Techniques Used to Derive Ocean Surface Winds. Technical Note/NMC Office Note No. 330, 34pp.

No. 15. Gemmill, W.H., T.W. Yu, and D.M. Feit 1987: Performance Statistics of Techniques Used to Determine Ocean Surface Winds. Conference Preprint, Workshop Proceedings AES/CMOS 2nd Workshop of Operational Meteorology. Halifax, Nova Scotia., 234-243.

No. 16. Yu, T.W., 1988: A Method for Determining Equivalent Depths of the Atmospheric Boundary Layer Over the Oceans. Journal of Geophysical Research. 93, 3655-3661.

No. 17. Yu, T.W., 1987: Analysis of the Atmospheric Mixed Layer Heights Over the Oceans. Conference Preprint, Workshop Proceedings AES/CMOS 2nd Workshop of Operational Meteorology, Halifax, Nova Scotia, 2, 425-432.

No. 18. Feit, D. M., 1987: An Operational Forecast System for Superstructure Icing. Proceedings Fourth Conference Meteorology and Oceanography of the Coastal Zone. 4pp.

No. 19. Esteva, D.C., 1988: Evaluation of Priliminary Experiments Assimilating Seasat Significant Wave Height into a Spectral Wave Model. Journal of Geophysical Research. 93, 14,099-14,105

No. 20. Chao, Y.Y., 1988: Evaluation of Wave Forecast for the Gulf of Mexico. Proceedings Fourth Conference Meteorology and Oceanography of the Coastal Zone, 42-49

No. 21. Breaker, L.C., 1989: El Nino and Related Variability in Sea-Surface Temperature Along the Central California Coast. PACLIM Monograph of Climate Variability of the Eastern North Pacific and Western North America, Geophysical Monograph 55, AGU, 133-140.

LIST OF ABBREVIATIONS

TB:	brightness temperature
NN:	neural network
NN1:	neural network for clear conditions - see Table 4
NN2:	neural network for cloudy conditions - see Table 4
NN3:	neural network for cloudy conditions with 5 inputs - see Table 4
NN4:	neural network for cloudy conditions with 6 inputs - see Table 4
NN5:	neural network for clear plus cloudy conditions - see Table 4
NN6:	"all-weather" neural network - see Table 4
NN7:	"all-weather" neural network with 6 inputs - see Table 4
NDBC:	National Data Buoy Center
DMSP:	Defense Meteorological Satellite Program
SSM/I:	Special Sensor Microwave Imager
GSW:	Goodberlet, Swift and Wilkerson (1989) - see References
GS:	Goodberlet and Swift (1992) - see References
SBB:	Stogryn, Butler and Bartolac (1994) - see References
SL:	Schluessel and Luthardt (1991) - see References
NMC:	National Meteorological Center
V:	vertical polarization
H:	horizontal polarization
GHz:	10^{12} cycles/second
K:	degrees Kelvin

ABSTRACT

Brightness temperatures from the Special Sensor Microwave Imager(SSM/I) are being used routinely to estimate surface wind speeds over the open ocean. At least six algorithms have been developed since 1983 which convert the SSM/I brightness temperatures to surface wind speed. The empirical relationships that were first developed between brightness temperature and wind speed were linear. Subsequently, nonlinear SSM/I brightness temperature/wind speed algorithms were developed to improve the accuracy of the wind speed retrievals. Recently, Stogryn, Butler and Bartolac(SBB) developed an SSM/I wind speed retrieval algorithm using neural networks (NNs) as a basis. The improvement in wind speed retrieval accuracies they achieved for "clear" and "cloudy" conditions were remarkable (30% for clear conditions and ~250% for cloudy conditions). In applying these previous SSM/I wind speed retrieval algorithms, it has been necessary to impose a number of restrictions (i.e., rain flags) on the brightness temperatures that can be used in retrieving surface wind speeds under adverse atmospheric conditions where atmospheric moisture levels become higher. As a result, it has not been possible to make surface wind retrievals at speeds greater than 15-20 m/sec with acceptable accuracy using the existing algorithms.

As a starting point for the present work, we first reproduce the results of SBB for "clear" and "cloudy" conditions using the same data sets and identically-constructed NNs. We then proceed to extend the results of SBB by constructing and training a single NN which can be applied to both clear and cloudy conditions. This single network not only eliminates the problem of bridging the gap between the clear and cloudy regions, but it also provided the basis for developing a network which could be extended to atmospheric conditions where higher levels of moisture exist. As a result, NNs were trained to cover adverse atmospheric conditions considered by SBB to be beyond the region where useful retrievals could be obtained. Finally, an "all-weather" network was constructed and trained which yields a bias of -0.05 m/sec and an rms error of 1.65 m/sec over the entire range of conditions encountered in the data. This network performs as well on the previous clear and cloudy cases as the previous networks which were trained specifically for these conditions. This "all-weather" network was also applied separately to the data not considered by SBB which corresponded specifically to adverse atmospheric conditions, and yielded accuracies which were only slightly lower than for the previous case, suggesting that at least a weak wind speed signal from the ocean surface remained in the data. Although no rain flag criteria for this algorithm have yet been applied, the need for at least limited brightness temperature restrictions are clearly recognized. Also, it was found that by including brightness temperatures at 85 GHz, a frequency not normally employed in retrieving surface wind speeds from the SSM/I, a slight improvement in retrieval accuracy could be achieved for cloudy/adverse conditions.

1. INTRODUCTION

Accurate synoptic-scale wind measurements over the ocean surface are required for operational marine meteorology. In-situ marine wind reports are sparse and at best can only describe the large-scale flow patterns over the ocean. Over the past 15 years, passive microwave radiometry has been used with increasing success to infer wind speeds within the marine boundary layer. The Scanning Multichannel Microwave Radiometer flown aboard the Seasat-A satellite demonstrated that representative near-surface measurements of wind speed could be made over the ocean (e.g., Wentz et al., 1986). More recently, the Special Sensor Microwave/Imager (SSM/I) flown aboard the Defense Meteorological Satellite Program's (DMSP) polar-orbiting satellites is being used to estimate boundary layer wind speeds for operational use over the ocean.

A number of algorithms have been developed which convert the various SSM/I channel outputs to surface wind speed. The original D-matrix algorithm used to estimate wind speed was based on a linear combination of SSM/I channel outputs and required nine sets of latitude and time dependent coefficients for its application (Lo, 1983). Goodberlet et al. (1989) improved this approach by developing a single algorithm (GSW) which could be applied globally. This algorithm also met specified accuracy criteria (2 m/sec between 3 and 25 m/sec) under rain-free and low moisture conditions. According to Goodberlet et al., however, this algorithm deteriorates rapidly in areas where rain and heavy cloud cover occur. Schluessel and Luthardt (SL; 1991) derived a relationship between the SSM/I channel outputs and wind speed similar to that obtained by Goodberlet et al. using a slightly different combination of channel outputs. Validation of their algorithm, however, was limited to observations from the North Sea. Wentz (1992) developed a physically-based approach to estimate surface wind speeds from the SSM/I quite different from those of Lo, Goodberlet et al., and Schluessel and Luthardt. Wentz also found that it may be

possible to estimate wind direction as well as wind speed using data from the SSM/I. However, Wentz's approach requires several external inputs not available in the SSM/I data stream.

Because of the high moisture/rain limitation, Goodberlet and Swift (GS; 1992) modified the original GSW algorithm due to its limitations in the presence of rain or high atmospheric moisture. More recently, Stogryn, Butler, and Bartolac (SBB; 1994) applied neural networks (NNs) to the problem of estimating surface wind speed from SSM/I data. The improvement in wind speed retrieval accuracy for clear conditions was approximately 30% and for higher moisture/higher wind speed conditions, the improvement was far greater compared to the currently-operational algorithm of Goodberlet et al. (1989) .

The results obtained by SBB in using NNs as a basis for improving the accuracy of SSM/I-derived wind speeds are impressive. However, the application of NNs to practical problems in meteorology and oceanography is relatively new. Moreover, SBB constructed and trained two separate NNs, one for clear conditions and a second for cloudy conditions, a situation which could lead to uncertainties in the region that separates these two regimes. Like GSW, SBB did not consider high moisture cases, a limitation which creates gaps in the wind speed fields which are retrieved. As a result, it was our intent to explore ways of further improving SSM/I wind speed retrieval accuracy, including the development of a single NN that could be used to retrieve surface wind speeds over a wider range of atmospheric conditions. The purpose of this study is to first document our work in reproducing the results of SBB and then to present new results which provide the basis for additional improvements to SSM/I wind speed retrievals using NNs. We give particular attention to those results which lead to the development of a single "all-weather" NN algorithm for operational SSM/I wind speed retrievals.

The text is organized as follows. Section 2 contains a brief introduction to the theoretical background appropriate to this study. Section 3 contains a brief

description of the SSM/I instrument. Section 4 summarizes previous algorithm development for estimating SSM/I wind speeds with corresponding rain flag/brightness temperature discriminants. Section 5 describes the data sets that were used in this study. Section 6 describes our work in reproducing the results of Stogryn et al. Section 7 describes our results in attempting to improve upon the results of Stogryn et al. using different NNs. Section 8 contains operational results at NMC using the NN presented in Section 7. Finally, section 9 contains a discussion and our conclusions.

2. THEORETICAL BACKGROUND

The composite brightness temperature (TB) signal received by a satellite radiometer at microwave frequencies can be expressed in simplified form as

$$T_0 = \varepsilon\ T_1 e^{-\tau} + T_2 + (1-\varepsilon)T_3 e\ + (1-\varepsilon)T_4 e^{-2\tau} \qquad (1)$$

where T_1 represents the surface temperature, ε, the surface emissivity, τ, the atmospheric transmissivity, T_2 and T_3, the TB contributions from the atmosphere, and T_4, the TB contribution from space. T_0 and ε are both functions of wavelength, polarization, and satellite zenith angle. The first term on the right-hand side of (1) represents emission from the ocean surface modified by atmospheric absorption, the second, upwelling radiation from the atmosphere, the third, reflected downwelling radiation modified by atmospheric absorption, and the fourth, reflected radiation from space modified by two-way absorption through the earth's atmosphere. T_2 may represent the dominant contribution to T_0 in the presence of rain, high humidity, or clouds, making it difficult or impossible to distinguish contributions from the other sources. Since absorption equals emission under the conditions of thermodynamic equilibrium, it follows that the term $(1 - \varepsilon)$ corresponds to the surface reflectivity. Finally, the relationships between T_0, the composite TB, and microwave frequency, polarization, and sensor viewing geometry are complicated and often create problems for the instrument designer and for the data analyst. To pursue this area in greater detail, see Swift (1990).

For inferring wind speed at the ocean surface, the surface emissivity, ε, is the single most important parameter. Winds act on the ocean surface to generate surface waves which increase in amplitude with increasing wind speed. As the waves grow, roughness elements associated with these waves likewise increase. Eventually, the waves begin to break forming whitecaps and foam. Because surface roughness and foam tend to scatter the emitted surface radiation, the

surface reflectivity decreases which in turn increases the surface emissivity. Thus, the surface contribution to T_0 increases as wind speed increases. Before the waves break, it is the surface roughness that produces the TB dependence on wind speed but when wave breaking occurs and foam is produced, a different mechanism for increasing surface emissivity takes place. Foam is a combination of air and water. Because this mixture has a lower reflectivity than pure water, it has a higher emissivity. As shown by Swift (1990), the TB contribution from a partially foam-covered surface can be expressed as

$$T_b = (1-\alpha_f)\varepsilon T + \alpha_f T \qquad (2)$$

where T is the temperature of the water/surface foam combination and α_f is the fraction of the satellite viewing area covered by foam. Since the area covered by foam increases with increasing wind speed, we again have a mechanism for establishing a TB dependence on wind speed. Ultimately, when wind speeds reach the point where the entire ocean surface is foam-covered, saturation of the TB signal from the surface occurs and the relationship breaks down. In such cases, it is likely that atmospheric contributions to the satellite-observed TB field will most often obscure any contributions from the ocean surface. Although it may be difficult to estimate surface wind speeds under such adverse oceanic/atmospheric conditions, it may not be impossible as shown by Black and Swift (1984), who were able to measure surface wind speeds up to 70 m/sec in rain rates of at least 50 mm/hr using a microwave radiometer aboard an aircraft.

There are several reasons why the overall relationship between satellite TB and surface wind speed is expected to be nonlinear and further, that the degree and character of nonlinearity may, in fact, change over the dynamic range of wind speeds encountered. First, different mechanisms are responsible for increasing surface emissivity depending on whether or not foam is present, and second, a power law relationship exists between foam cover fraction and wind speed (Stogryn,

1972). These combined dependencies have important implications for the type of modeling approach that is used to establish empirical relationships between SSM/I-observed TBs, and in situ wind speeds.

3. INSTRUMENT DESCRIPTION

The SSM/I is a microwave radiometer flown aboard the DMSP polar-orbiting satellite. The first instrument was flown aboard the DMSP F8 satellite in 1987. Today, the current spacecraft in the sequence of DMSP satellites are designated F10 and F11. The orbit of the DMSP satellite is circular and sun-synchronous. The spacecraft altitude is approximately 835 km with an orbital angle of inclination relative to the equatorial plane of approximately 99 degrees.

The SSM/I is a seven-channel, four-frequency linearly polarized passive microwave radiometer. This instrument receives vertically polarized radiation at 22.2 GHz and vertically and horizontally polarized radiation at 19.3, 37.0, and 85.5 GHz. The SSM/I antenna beam pattern produces a conical scan. The SSM/I viewing angle relative to nadir is 45 degrees (following the spacecraft) with observations taken ± 51 degrees about the aft direction. The active portion of the SSM/I viewing area or scan covers a swath of approximately 1400 km. Adjacent satellite passes are approximately 2500 km apart at the equator, leaving gaps ~ 600 km wide between adjacent orbits. The gap locations are not fixed because the subsatellite ground track repeats itself on an approximate 16-day cycle. With two satellites in orbit, the ground coverage is almost complete on a daily basis. Orbital coverage for the DMSP F10 and F11 satellites is shown in Fig. 1. At 85 GHz, 128 uniformly-spaced samples are taken over the entire 1400 km scan yielding a nominal spatial resolution of 12.5 km. At the three lower frequencies, 64 samples are taken over the entire scan, yielding a nominal resolution of 25 Km. For further details on the SSM/I instrument, see Hollinger et al. (1990).

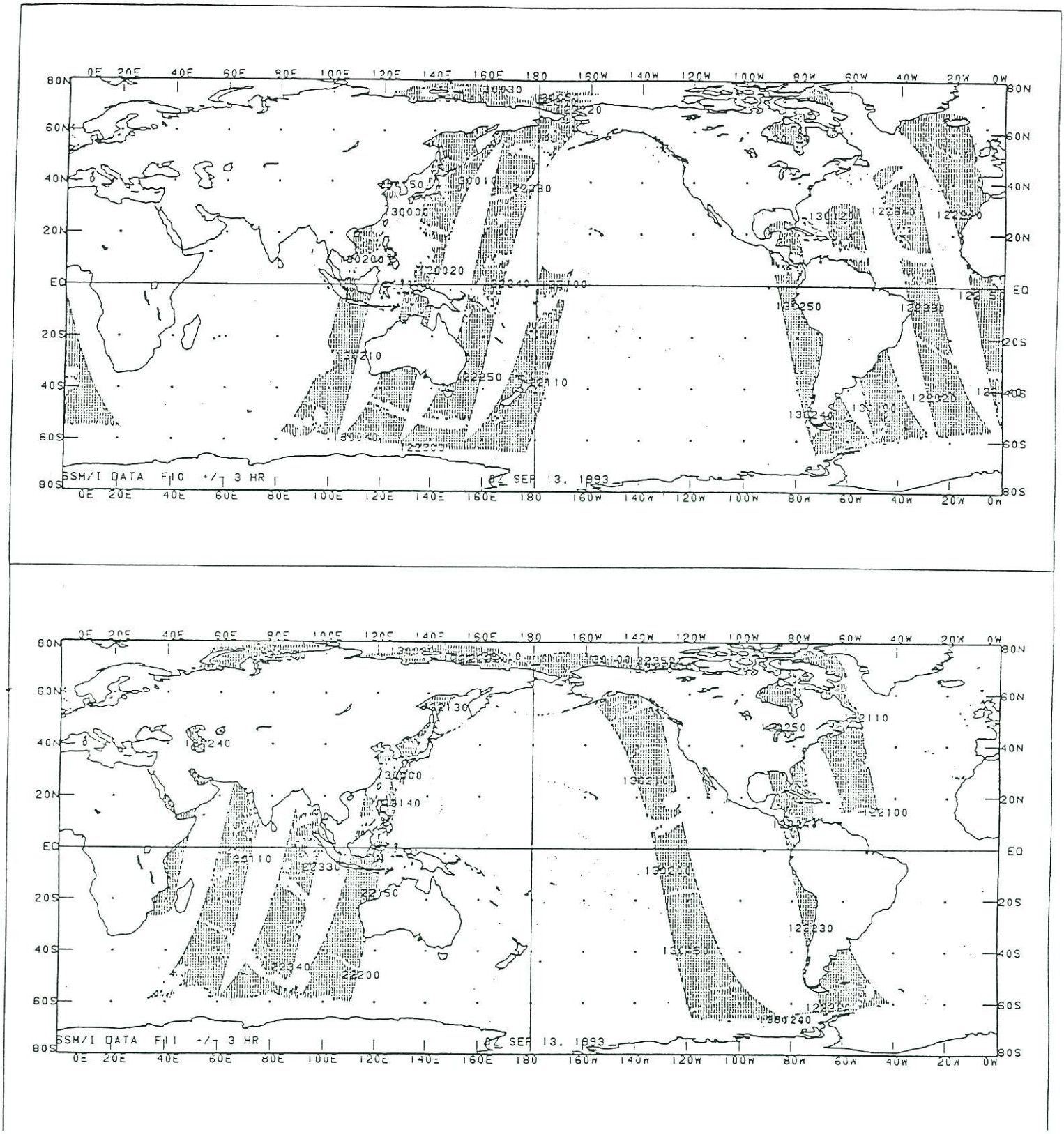

Fig. 1. Orbital coverage for the DMSP F10 and F11 satellites

4. PREVIOUS ALGORITHMS AND RAIN FLAG CRITERIA

The SSM/I retrieval problem may be expressed formally as:

$$W = F(t_1, t_2, ..., t_7) \qquad (3)$$

where W is the retrieved wind speed, t_1, ..., t_7 are channel TBs, and F is a complicated, and most likely, nonlinear transfer function (see previous section) which represents all of the processes that influence the wind speed signal from its emission at the ocean surface to its manifestation as a TB signal at the output of the SSM/I.

Because the physics that defines these processes is only partially understood, it is difficult to create a theoretical model for F. As a result, most of the retrieval algorithms that have been developed are essentially empirical. Furthermore, these models are often linear.

We review here a number of algorithms which have been used to retrieve surface wind speed based on the TBs and polarizations available from the SSM/I. Each of these algorithms has been developed for specific atmospheric/oceanic conditions. TBs from the SSM/I are used as a basis for discriminating between various levels of atmospheric moisture and thus we include the appropriate TB discriminants (i.e., rain flag criteria) that were used or recommended in each case.

We start with the original D-matrix algorithm given by Lo (1983), where the surface wind speed, W, is given as

$$W = C_0(i) + C_1(i)TB19H + C_2(i)TB22V + C_3(i)TB37V + C_4(i)TB37H \qquad (4)$$

This relationship gives the wind speed in m/sec at a height of 19.5 m for TBs expressed in degrees K. The TB's represent the brightness temperatures at the

SSM/I frequencies and polarizations indicated, and the C_i's are the D-matrix coefficients which are a function of latitude and season. Following Lo, 11 sets of coefficients, only 9 of which are unique, are required to span the entire range of latitudes and seasons. In this case, the relationship between wind speed and TB is linear. Equation (4) corresponds to a linear (location and time dependent) model for the transfer function F in (3), and, as indicated, uses only four of the seven TBs which are available.

The corresponding rain flag criteria are

If TB19H > 190 K

or $\Delta_{37} < 25$ K, where Δ_{37} = TB37V - TB37H

then rain is possible and the rain flag is set equal to 1.

If $\Delta_{37} < 10$ K

heavy rain is indicated and the rain flag is set equal to 2.

An improved global D-matrix algorithm (i.e., single equation) was developed by Goodberlet, Swift and Wilkerson (1989). The wind speed, W, is given in m/sec as

$$W = 147.90 + 1.0969\ TB19V - 0.4555\ TB22V - 1.7600\ TB37V + \\ + 0.7860\ TB37H \qquad (5)$$

where the coefficients were determined using data from the DMSP F8 spacecraft and the height of the wind speed is 19.5 m. Again, the relationship between wind speed and TB is linear. This algorithm (5) corresponds to a more general linear model for the transfer function, F. Today, this algorithm is being used to retrieve surface wind speeds over the ocean on an operational basis by the Navy, the Air Force, and NMC.

The rain flag criteria for this algorithm are:

Rain Flag 0: $\Delta_{37} > 50$ K

TB19H < 165 K yields an error < 2 m/sec [3].

Rain Flag 1: 37 K < Δ_{37} <50 K

TB19H > 165 K yields an error of 2-5 m/sec.

Rain Flag 2: 30 K < Δ_{37} < 37 K yields an error of 5-10 m/sec.

Rain Flag 3: Δ_{37} < 30 K yields an error > 10 m/sec.

Because the Goodberlet et al. (1989) algorithm produced poor results under adverse weather conditions (i.e., clouds, water vapor and/or rain), Goodberlet and Swift (1992) modified their previous algorithm to produce better results for water-laden atmospheres. If we refer to (5) as "GSW", then the modified equation can be expressed as

$$W_{GS} = (W_{GSW} - 18.56\,\alpha) / (1. - \alpha) \qquad (6a)$$

where W_{GSW} is the wind speed from (5), and α is given by

$$\alpha = (30.7/\Delta_{37})^4 \qquad (6b)$$

This modified version has the undesirable property that when Δ_{37} approaches 30.7 K, W has a singularity and thus the expression becomes meaningless in this region. This is unfortunate since TB differences at 37 GHz (i.e., between the V and H polarizations) in this range often correspond to higher moisture regimes

[3]Note that in GSW (1989), this TB criteria is given as TB19H < 165 K, whereas in GS (1992) it is given as TB19H > 165 K. The first criteria appears to be correct and is thus given here.

which may be of interest. Unlike its predecessors, however, the relationship between wind speed and TB is nonlinear with respect to the two TBs at 37 GHz (H and V), as indicated in (6). This modified algorithm, however, has not been adopted for operational use.

Schluessel and Luthardt (1991) present another algorithm for calculating surface wind speeds from the SSM/I. Simulated TBs are obtained by calculating the radiative transfer for the SSM/I channels applied to a global set of vertical profiles of temperature and humidity with the addition of artificially-introduced multilayer clouds. Randomly-generated sea surface temperatures and wind speeds at 10 m are included. The wind speeds were uniformly distributed between 0 and 30 m/sec. Schluessel and Luthardt use these results together with a subsequent regression analysis to construct a new wind speed algorithm based on the available TBs and polarizations from the SSM/I. Three alternate regression relationships are given. Based on surface-truth wind speed comparisons in the North Sea, their third algorithm produces the best results and is given below:

$$W = 149.0 + 0.8800\ TB19V - 0.4887\ \Delta_{19} - 0.4642\ TB22V - 0.7131\ TB37V - 0.4668\ \Delta_{37} \qquad (7)$$

where $\Delta_{19} = TB19V - TB19H$

Wind speed is calculated in m/sec and TBs are in degrees K. This retrieval scheme is also linear and very similar to that of Goodberlet et al. (1989) and uses five (vs. four) TBs. It also produces retrieval accuracy similar to GSW (rms differences of 2.0 m/sec). However, it was only verified in one area, the North Sea.

The only rain flag criteria used by SL was

$$5\ K < TB85V - TB37V < 55\ K,$$

where SSM/I TBs that fell outside this range were excluded due to rain. Only 2% of their data were excluded on this basis.

Wentz (1992) presents a different approach for estimating SSM/I surface wind speeds. Here, the TBs at 37 GHz (H and V) are equated to separate functions of the desired wind speed, W (at 19.5 m), and the atmospheric transmittance, τ

$$TB37V = F_V(W, \tau) \quad (8a)$$

$$TB37H = F_H(W, \tau) \quad (8b)$$

The model functions, F_V and F_H are expressed in radiative transfer form for a dry, nonscattering atmosphere. Several of the required inputs to the model equations such as sea surface emissivity, sea surface temperature, and effective air temperature must be calculated separately or approximated from climatology. The calculation of surface emissivity is non-trivial. Once the model equations for F_V and F_H are specified, (8a) and (8b) can be solved using a numerical scheme such as Newton's method. The final solution for W is obtained by inverting (8) and then iterating until the solution for W converges. Because of the need for external information and difficulties that arise in estimating these model functions, this approach does not appear to be well-suited for rapid, real-time applications.

Because rain produces large variations in atmospheric TB tending to obscure the weaker surface wind speed signals, Wentz indicates that SSM/I wind speed retrievals are only valid when the vertically-integrated absorption due to liquid water at 37 GHz does not exceed 0.044 napers. A method for estimating this quantity is given by Wentz.

A recent algorithm for estimating surface wind speeds from the SSM/I using neural networks (NNs) has been presented by Stogryn, Butler, and Bartolac (1994). The SSM/I TB/buoy wind speed matchup database that was

used in their study is described in the next section. The SSM/I channels used to train the NNs were 19.3 GHz(V), 22.2 GHz(V), 37.0 GHz(V) and 37.0 GHz(H). Separate networks were constructed for clear and cloudy conditions to distinguish between rain-free and light-rain situations. The NN equations take the following form

$$W = Net(\mathbf{T}) \tag{9}$$

where the TB input vector $\mathbf{T} = \{t_1, t_2, t_3, t_4\}$ = {TB19V, TB22V, TB37V, TB37H}, and Net is a nonlinear operator (see Section 6 for a detailed description). The NN algorithm (9) corresponds to a very general nonlinear model for the transfer function, F in (3), and does not require any a priori knowledge about the particular form of the input/output relationship. The rain flag criteria used by SBB to distinguish between clear and cloudy conditions are presented in the next section.

The NN approach of SBB shows a 30% improvement in wind speed retrieval accuracy over GSW for clear conditions and roughly a 250% improvement for cloudy conditions. However, the use of two different NNs, which corresponds to a piecewise approximation of the transfer function, leads to a region of discontinuity between the clear and cloudy regimes. Furthermore, their approach was not applied to higher moisture levels beyond the cloudy regime. In what follows, we strive to surmount these limitations.

5. THE DATA USED FOR ALGORITHM DEVELOPMENT AND TESTING

a. SSM/I/Buoy Matchups

The data used in this study consist of matched pairs of SSM/I TBs and NDBC buoy wind speeds acquired at closely coincident times and locations over the open ocean (and at least 100 km away from land). The TBs were acquired from the SSM/I flown on the DMSP F8 satellite. Matchups were produced only when the SSM/I retrievals were within 25 km of the buoy location and the time of satellite data acquisition was within 30 minutes of the buoy observation. In each case, wind speeds have been adjusted to a standard height of 19.5 m. These data were provided to us by G. Poe. They are identical to the data used by SBB (1994) and were originally compiled by GSW (1989).

Each SSM/I/buoy matchup consists of (i) seven SSM/I TBs at 19.3 GHz (H and V), 22.2 GHz (V), 37.0 GHz (H and V), and 85.5 GHz (H and V), and (ii), the corresponding buoy wind speed. These matchups are divided into two sets; the first set for training and the second set for testing. During the course of the study, SBB reversed the role of the training and test data sets in order to maximize the amount of information that could be extracted from them. We have done the same. SBB subdivided each set into three subsets. The first subset includes all matchups where the SSM/I TBs satisfied the following condition,

$$\Delta_{37} > 50 \text{ K}.$$

Note that this discriminant is not as restrictive as the GSW (1989) rain flag zero criteria which, in addition to the above, also requires that TB19H < 165 K. This subset (subset #1 in Table 1) corresponds to "clear" conditions, according to the terminology adopted by SBB. The remaining matchups where $\Delta_{37} \leq 50$ K,

were further subdivided into two groups. The first group meets the following TB criteria,

$\Delta_{37} \leq 50$ K
T19V < T37V
T19H $\leq$ 185 K
T37H $\leq$ 210K

which corresponds to "cloudy" conditions, following SBB (subsets #2 in Table 1). The remaining matchups constitute subsets #3 (see Table 1), corresponding to "very cloudy" conditions. According to SBB, for subset #3, " wind speed effects on TB are so overshadowed by atmospheric attenuation that retrievals should not be attempted". The first TB discriminant corresponds to the GSW (1989) rain flag one criteria but the other discriminants do not correspond to any of the higher GSW rain flag criteria (and no explanation for how they were determined was provided). Thus, SBB formed three subsets, the first and second corresponding roughly to clear and cloudy conditions, respectively, and implicitly, a third, which we call "very cloudy" conditions. Loosely, the term clear corresponds to low wind speed/low moisture conditions whereas cloudy corresponds to higher wind speed/higher moisture conditions, and finally, the label "very cloudy" corresponds to high wind speed/high moisture conditions where the distinctions between categories are based on the previous TB discriminants.

Table 1 shows the number of matchups contained in each of the subsets used for training and for testing by SBB, and by us. SBB constructed separate NNs for the clear and the cloudy cases; however, due to the expected problems arising from increased atmospheric attenuation at the higher wind speeds, they did not attempt to construct a NN for the very cloudy case.

Table 2 shows the means and standard deviations stratified by subset (i.e., clear, cloudy, and very cloudy) for the buoy wind speeds that were used in creating the matchups. Figure 2 shows that the frequency distribution of wind speed for training and testing are similar. In both cases, these distributions are nonuniform; the maximum number of observations peak in the 4 - 7 m/sec range, and no observations occur beyond ~18 m/sec. The lack of observations at the higher wind speeds has important implications for our ability to adequately train a NN to retrieve wind speeds in this region.

Table 1. The number of matchups in subsets # 1,2,3,4 in the training and test sets.

Subset	Training set	Test set
# 1 or "clear"	1684	1673
# 2 or "cloudy"	220	238
# 3 or "very cloudy"	75	68
# 4 or "clear + cloudy"	1904	1911
Total (# 5)	1979	1979

Table 2. Statistics for buoy wind speeds.

Subset	Training set		Test set	
	Mean	σ	Mean	σ
# 1	6.41	3.01	6.46	3.08
# 2	8.89	3.57	9.04	3.39
# 3	8.03	3.19	7.86	3.55
Total (# 5)	6.75	3.19	6.82	3.25

min 0.13 max 21.15 min 0.22 max 19.3

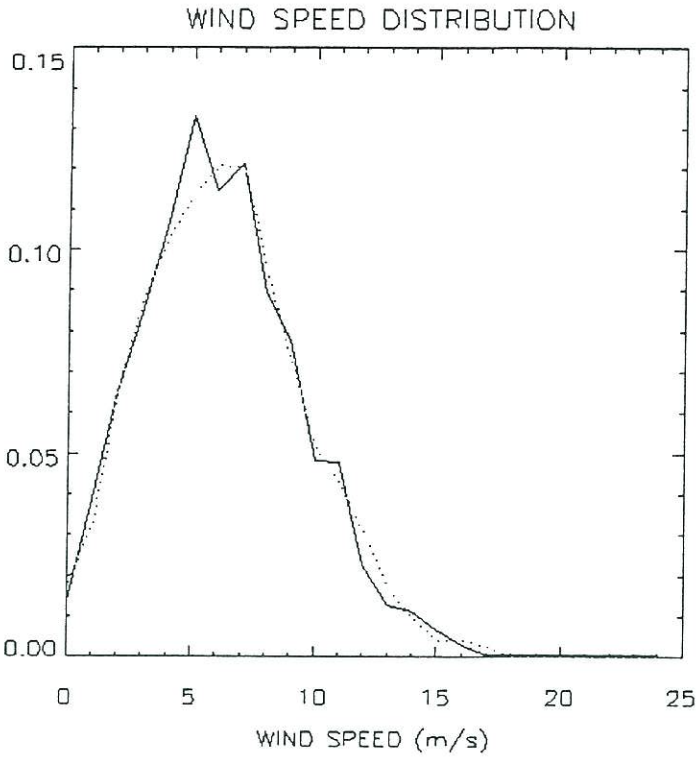

Fig. 2. Normalized wind speed distribution for the training (solid) and test (dotted) data sets.

Table 3 presents the means and standard deviations separately for each SSM/I TB channel for the training and test data. Because these statistics vary significantly from one channel to the next, this table emphasizes the need to rescale or normalize the data before any NN calculations are undertaken.

Table 3. Brightness temperature statistics for SSM/I data.

Channel	Training set		Test set	
	Mean	σ	Mean	σ
T19V	196.5	13.9	196.6	14.3
T19H	132.4	22.7	132.7	23.3
T22V	219.2	20.8	219.4	21.1
T37V	214.8	10.5	215.0	10.8
T37H	157.4	20.3	157.8	21.0
T85V	254.2	14.4	254.2	13.5
T85H	222.8	25.4	223.1	25.5

b. NN classification

In this study, we constructed, trained, and tested a number of different NNs. Different subsets were used for training and testing these NNs; in some cases, the number of inputs was varied. Their nomenclature and certain characteristics are summarized in Table 4.

Table 4. NNs examined in the study.

Abbr.	Atmospheric conditions	# of inputs	Inputs	Training set
NN1	Clear only	4	TB19V, TB22V, TB37H,V	# 1
NN2	Cloudy only	4	Same as for NN1	# 2
NN3	Cloudy only	5	Same as for NN1 plus TB19H, TB85H or TB85V as the 5th input	# 2
NN4	Cloudy only	6	Same as for NN1 plus TB85H,V as the 5th and 6th inputs	# 2
NN5	Clear+Cloudy	4	Same as for NN1	# 1 + # 2
NN6	"All-Weather"	4	Same as for NN1	# 1 + # 2 + # 3
NN7	"All-Weather"	6	Same as for NN4	# 1 + # 2 + # 3

6. REPRODUCING THE RESULTS OF SBB

In order to reproduce the results of SBB and to make our findings directly comparable with theirs, we have adopted the same NN design or architecture. Thus, we have constructed feed-forward, fully-connected NNs which employ back-propagation, a technique commonly used for training multilayer NNs (e.g., Wasserman, 1989). These NNs contain three layers, an input layer, one hidden layer, and an output layer (Fig. 3).

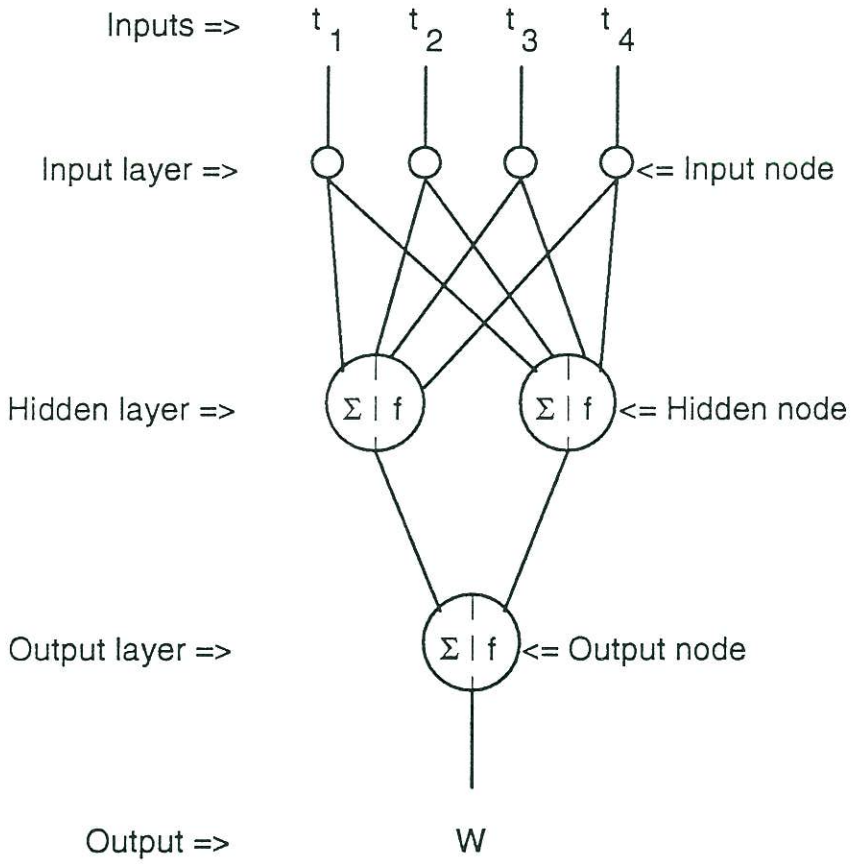

Fig. 3. The basic architecture of the four-input NNs used in this study.

The input layer (layer 0) has four nodes (n = 4) which simply pass the input TBs in degrees K (i.e., 19.3 GHz(V), 22.2 GHz(V), 37.0 GHz(V), and 37.0 GHz(H)), to the hidden layer (layer 1). The hidden layer has two processing elements or nodes (m = 2). Since these NNs are fully connected, each input is connected to each of the nodes in layer 1. The hidden layer is followed by a final output layer (layer 2) which contains one node. Both nodes in the preceeding layer (layer 1) are connected to the output node. At the nodes in layers 1 and 2, linear combinations of the outputs from the nodes in the previous layers (layers 0 and 1) are formed. Thus, we can express the combined input to node j in layer 1 as

$$y_i = \sum_{j=1}^{n} \Omega_{i,j} t_j + \mathrm{B}_i \qquad (10)$$

where the t_j are the four input TBs, the $\Omega_{i,j}$ are weights, the B_i are biases, and j = 1,2 (nodes of hidden layer). To transform this combined input into an output at each node, a nonlinear transfer function, often called a squashing function, is employed. Thus, the output for the i-th node can be expressed as

$$x_i = f(y_i) \qquad (11)$$

where *f* represents the squashing function. In our case, *f* was chosen to be

$$f(x) = \tanh(x) \qquad (12)$$

although the final results are not usually strongly dependent on the exact choice of the squashing function. However, it is essential that this function has a nonlinear transfer characteristic in order for the NN to represent input/output relationships which are inherently nonlinear. Also, this function must be bounded and monotonically increase over the range of the independent variable. A bias term, B_i, is included in (10) to center the squashing function about the ordinate, an addition which makes the training

process more efficient. The output of hidden node x_i provides the input to the output node, which in turn produces the NN output:

$$Net = b + af(\sum_{i=1}^{m} \omega_i x_i + \beta) \qquad (13)$$

where the ω_i are the weights, β is the bias, and *a* and *b* are scaling factors.

Once the training is complete and the weights have been determined, the desired wind speed, W(m/sec), is calculated as

$$W = Net\ (\mathbf{T}) \qquad (14)$$

where **T**, as before, is the input vector of TBs.

Before network training can begin, initial weights for each of the connections within the network must be specified. Often, these weights are chosen randomly (e.g., Wasserman,1989). However, other weight initialization schemes are used (e.g., Wessels and Bernard, 1992; Nguyen and Widrow, 1990) and we have chosen one recommended by Nguyen and Widrow because it gives the most rapid convergence to a solution in our case. Next, the TB inputs are applied to the NN and the output wind speed, W, is calculated. This output is then compared to the observed or target wind speed, w, contained in the matchup. The function that was used to minimize the error was

$$E = \frac{1}{N} \sum_{i=1}^{N} (W_i - w_i)^2 \qquad (15)$$

where N is the number of matchups in the training set. E is often called the cost function.

The difference between the calculated wind speed and the target wind speed is fed back through the network and the weights at each node are changed in order to minimize the error. This process is called backpropagation and is repeated many times

until the error converges to an acceptably small value. Deciding when convergence to the minimum error or at least a near minimum has been achieved is one of the more difficult issues that face NN users and represents a problem in nonlinear optimization. Training takes place as the network is repeatedly exposed to matched pairs of SSM/I TBs and buoy wind speed. After each exposure, the weights and biases are adjusted in accordance with the following training rule (e.g., Simpson, 1990):

$$\xi_{new} = (1-\eta)\xi_{old} + \eta\Delta\xi \qquad (16)$$

where ξ is an adjusted weight or bias, and $\Delta\xi$ is a weight (or bias) increment calculated by the backpropagation algorithm,

$$\Delta\xi = -\frac{\partial E}{\partial \xi} \qquad (17)$$

where the partial derivative in (17) can be expressed in terms of the derivative of the squashing function f (Simpson, 1990). η is called the learning constant. The learning constant controls the rate at which the weights and biases are adjusted and has important implications for locating the solution during convergence and for the convergence rate itself. In our case, the learning constant was changed adaptively during training to accelerate the convergence process.

Once the network was constructed, training was undertaken first using the data originally designated for training by SBB and then tested on the data designated for testing. Then the roles of the training and test data sets were reversed following SBB. Before training was started, the TBs in each channel were rescaled so that the ranges of values between channels were similar. This rescaling was accomplished by normalizing the values in each channel based on the maximum and minimum values that occurred. During training, several hundred to several thousand iterations were required in order to achieve convergence. Because of the simple NN architectures employed, CPU times were minimal (< 5 minutes in all cases for a VAX workstation model 4000.60).

a. Clear conditions

First, we present the results for the clear/low moisture conditions (Δ_{37} > 50 K). Table 5 shows the biases, rms differences, correlation coefficients and skewnesses for (i) the original GSW (1989) algorithm, (ii) the modified GS (1992) algorithm, (iii) the SBB (1994) NN algorithm, and (iv), our own NN algorithm (NN1) for both the training and the test data sets. Standard definitions for each of the statistics were adopted (e.g., Ostle and Mensing,1975). The statistics are based on the differences between the algorithm-derived, and the observed (buoy) wind speeds. Each of the statistics shows that the NN-based algorithms outperform the GSW and GS algorithms. Also, the NN1 algorithm shows slight improvement over the SBB algorithm both in terms of the bias and the rms differences; however, the differences are small and it is difficult to determine their significance. What is significant in our view is that similar results were obtained using independently-constructed and trained NNs.

Table 5. Performance of different algorithms on the training and test sets for clear conditions (set # 1).

Algorithm	Bias	RMS	Corr. Coeff.	Skewness
Training set				
GSW	-1.0	2.02	0.866	-0.553
GS	-0.17	1.85	0.865	-0.617
SBB NN	-0.07*	1.41	0.885*	-0.360*
NN1	0.001	1.38	0.888	-0.219
Test set				
GSW	-1.1	2.13	0.869	-0.654
GS	-0.26	1.98	0.866	-0.764
SBB NN	0.1	1.41	0.890*	-0.211*
NN1	-0.02	1.40	0.891	0.073

* These values were not presented in SBB (see Stogryn et al., 1994), however, they were calculated during this study using the weights presented in Table 3 of SBB.

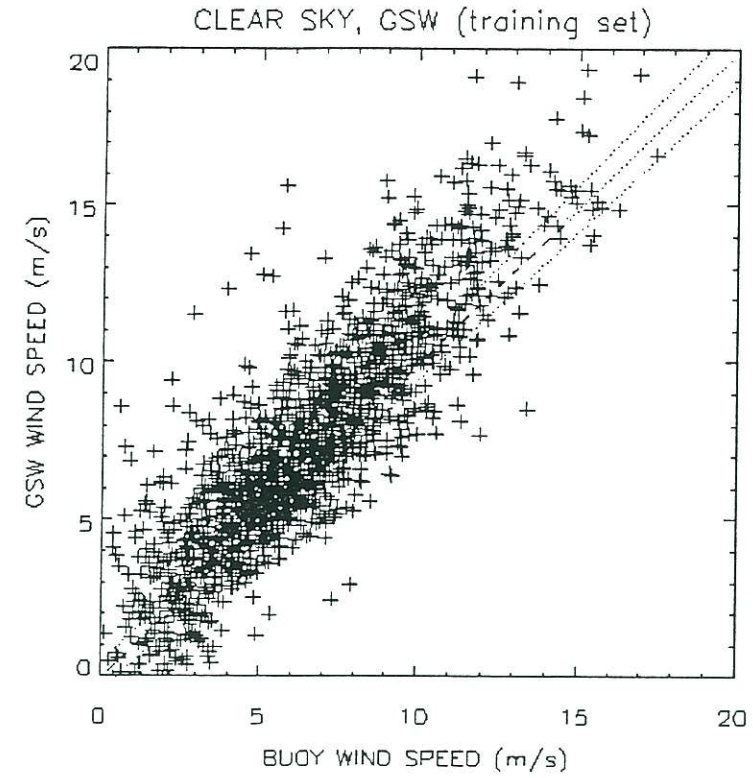

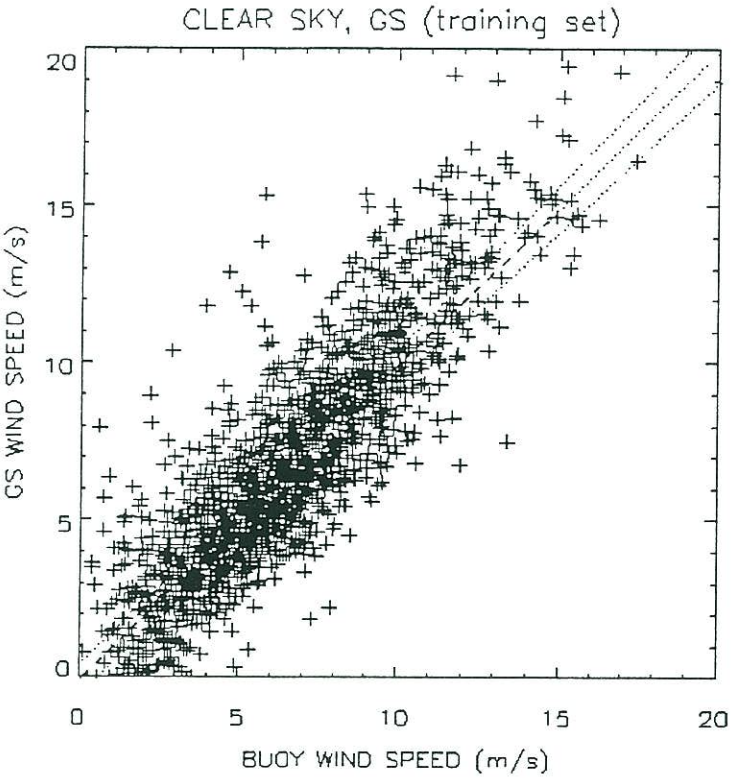

Fig. 4 (top) and Fig. 5 (bottom). Scatter plots for GSW and GS algorithms

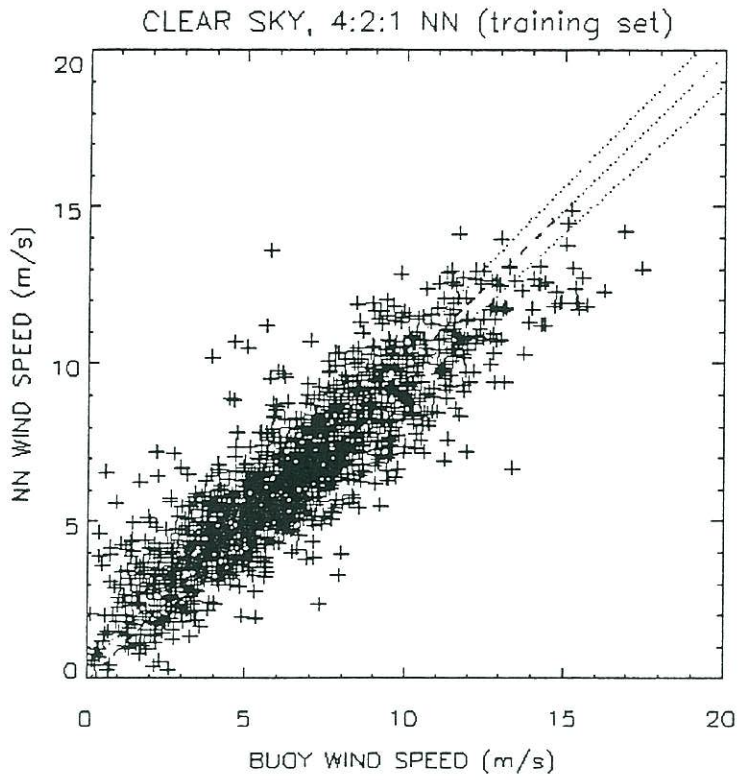

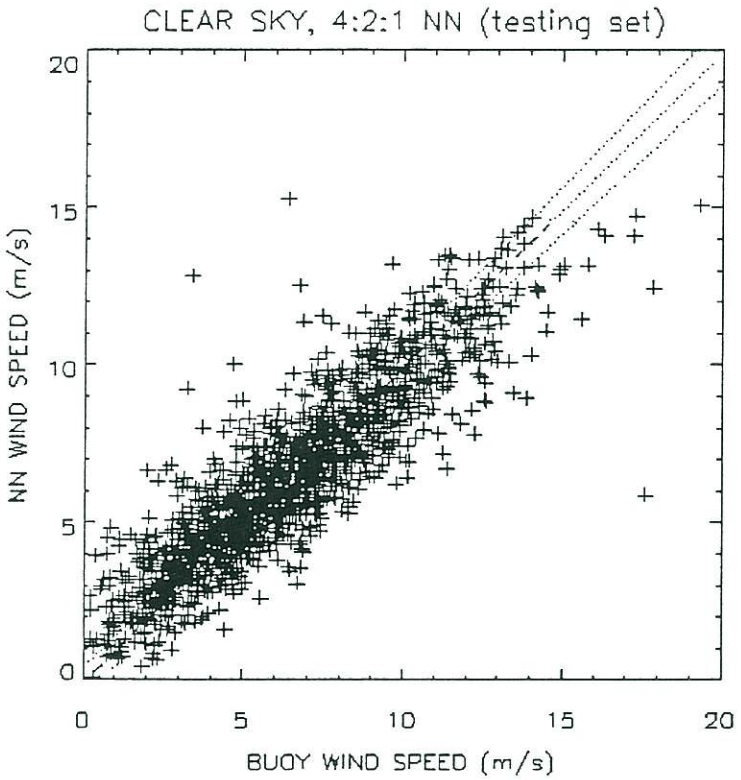

Fig. 6 (top) and Fig. 7 (bottom). Scatter plots for NN1 for the training and test sets.

Additional statistics are contained in Table 5 which we have calculated using the weights presented in SBB (1994). A comparison of our results with SBB show that they are consistently similar for the clear case. Consequently, in the following comparisons with the GSW and the GS algorithms, we include only our results since to continue including the results for the SBB NN would be essentially redundant. We also point out that SBB used only the bias and rms statistics for comparison whereas we include additional statistics (the correlation coefficient and skewness) and introduce several plots (scatter plots, wind speed distributions and wind speed error distributions) to provide a more complete basis for evaluating our results. We note that NN2 produces a much smaller bias and smaller skewness than SBB, a result that is most likely related to details of the training process and to the method of rescaling the TBs initially.

Figures 4-7 show scatter plots of SSM/I wind speed versus buoy wind speed for the (i) GSW, (ii) GS, and (iii), the NN1 algorithms, using the training data set. In these

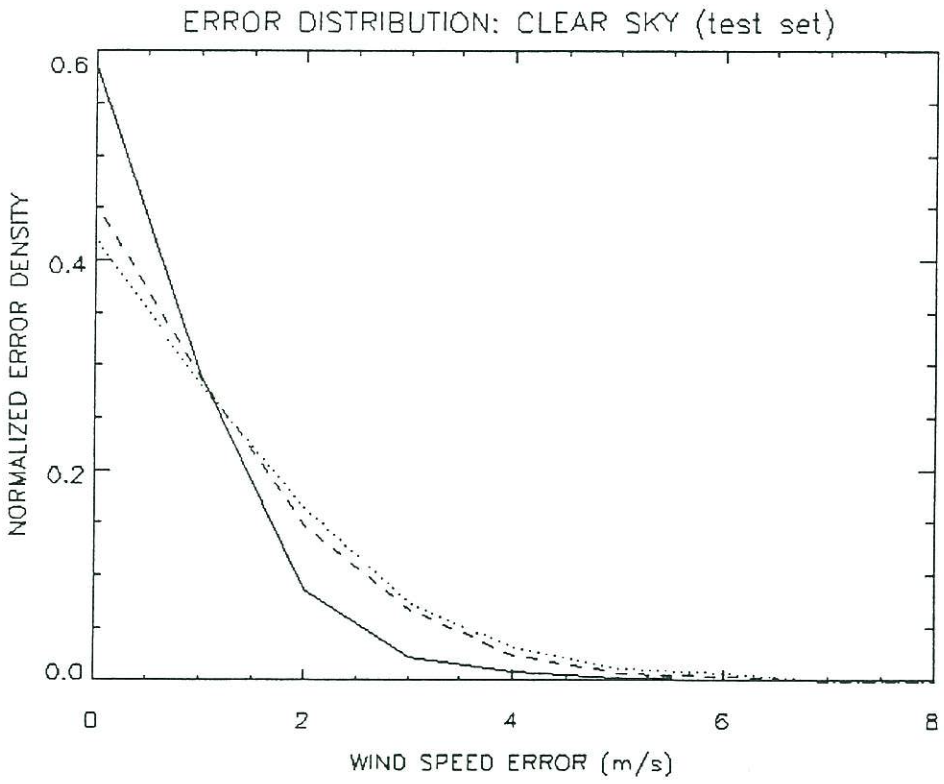

Fig. 8. Error distributions for NN1 (solid), GSW (dotted) and GS(dashed) for test data.

figures, the line $y = x$ indicates perfect agreement between the buoy observations and the SSM/I algorithm. The outer dashed lines provide a measure of uncertainty in the buoy observations themselves (Gilhousen,1986). For NN1, the scatter plots for the training and the test data sets are both shown to emphasize the similarity in performance of NN1 on independent data vs. the data it was trained on. Clearly, the NN1 plot shows less overall scatter and a better fit to the data. Figure 8 compares these algorithms by plotting the normalized error density (directly analogous to relative frequency in elementary statistics) for wind speed versus the error in wind speed itself. This plot indicates that the errors for NN1 are concentrated closer to the ordinate than the errors for GSW or GS, leading to a more peaked distribution with a shorter tail. The algorithms presented here can also be applied to the SSM/I TBs to reproduce the entire training and test data sets. Thus, statistics (i.e., the means and standard deviations) for the SSM/I-produced wind speeds can be compared directly with corresponding statistics for the observed wind speeds. Table 6 shows this comparison and includes the mean values for the wind speed squared as well, to emphasize the importance of the errors for the higher moments of wind speed (e.g., wind stress). The NN1 algorithm reproduces the mean values closely in each case. The GSW and GS algorithms overestimate the variance whereas NN1 underestimates the variance. We note, however, that GSW and GS tend to overestimate the variance more than NN1 underestimates it. The distributions of wind speeds for the SSM/I-derived winds and for the observed winds are plotted in Figure 9. The NN algorithm produces a closer fit to the observed distribution, particularly at wind speeds above 11 m/sec, than the other algorithms. Both the GSW and GS algorithms overestimate the tail of the wind speed distribution which produces large errors in the higher moments for wind speed (e.g., wind stress. For wind speed squared, the GSW algorithm produces an error of about 35% (see Table 6) and about 75% for the wind speed cubed (not shown).

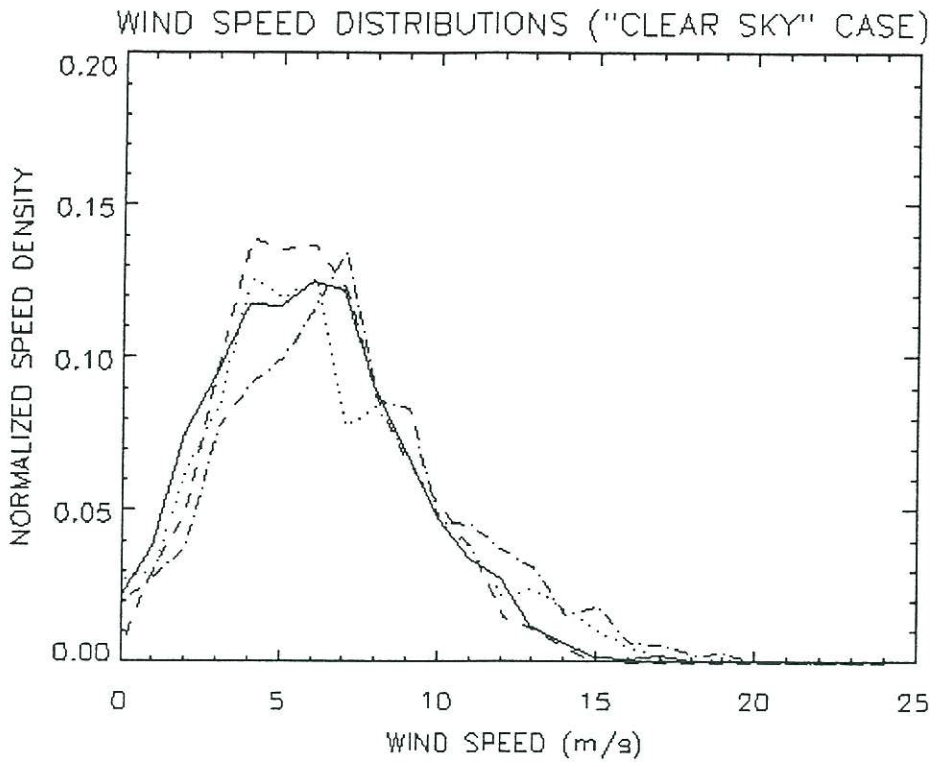

Fig. 9. Wind speed distributions for the clear case. Buoy winds (solid), NN (dashed), GSW (dotted) and GS (dot-dashed) - produced winds.

Table 6. Mean values and standard deviations for clear conditions (set # 1).

Source	Mean w	Mean w^2	σ
Training set			
Buoy data	6.41	50.1	3.01
GSW	7.39	67.0	3.52
GS	6.58	56.7	3.66
NN1	6.41	48.2	2.67
Test set			
Buoy data	6.46	51.2	3.08
GSW	7.52	70.4	3.73
GS	6.71	60.2	3.89
NN1	6.48	49.7	2.77

b. Cloudy conditions

Next, we show the results for cloudy conditions (subset # 2) using the TB discriminants of SBB, where

$\Delta_{37} \leq 50$ K

TB19V < TB37V

TB19H $\leq$ 185K

TB37H $\leq$ 210K

As indicated in the previous section, the first TB discriminant corresponds to the GSW rain flag zero criteria but the remaining TB discriminants were not obtained from GSW, but were adopted independently by SBB. Table 7 presents the same statistics that were given in Table 5 but for the cloudy case, for the GSW, the GS, the SBB, and NN2 (our NN for the cloudy case) algorithms for the training and test data sets. For the test data, GS performs poorly because some of the TB differences, i.e., Δ_{37}, are close to 30.7 K where this algorithm has a singularity. Consequently, the TBs in this region were removed and the results for GS recalculated. These results are shown just below the first table entry for GS and indicate considerable improvement. Again, the NN results of SBB and NN2 are similar and both show a large improvement over the GSW and the GS algorithms. We note, however, that NN2 produces a much smaller bias and a smaller skewness than SBB, a result most likely related to the training process and the method of rescaling the TBs initially.

Figs. 10-13 show scatter plots of SSM/I wind speeds versus buoy wind speeds for the GSW, the GS, and the NN2 algorithms using the training data set. Again, the NN2 algorithm (and presumably SBB), shows less scatter and a better fit to the data than the other algorithms. The normalized error density plot in Fig.14 shows that NN2 produces a distinctly sharper error distribution with a smaller tail than either GSW or GS. Table 8 shows the same statistics for the cloudy case that were shown in Table 6 for the clear case. The statistics for the SSM/I-produced, and the observed, wind speeds again

indicate for both data sets (i.e., training and test) that the NN reproduces the sample means closely whereas the others do not. Also, NN2 underestimates the sample variance whereas GSW and GS overestimate the variance, as before. Finally, the wind speed distributions in Fig. 15 show that the NN provides a closer fit to the

Table 7. Performance of different algorithms on the training and test sets for cloudy conditions (set # 2).

Algorithm	Bias	RMS	Corr. Coeff.	Skewness
Training set				
GSW	-4.0	5.13	0.608	-0.861
GS	-1.39	9.96	0.244	5.13
SBB NN	0.47*	2.39*	0.758*	-0.621*
NN2	0.006	2.30	0.765	-0.496
Test set				
GSW	-3.92	5.08	0.583	-1.845
GS	5.56	101.0	-0.006	14.66
GS(Δ_{37} >31)	-1.79	8.76	0.389	-7.9
SBB NN	0.5	2.39	0.712*	-0.802*
NN2(Δ_{37} >31)	0.2	2.05	0.801	-0.148
NN2	0.02	2.38	0.711	-0.578

* These values were calculated using the weights presented in Table 3 of SBB.

observed data than either the GSW or the GS algorithms, particularly at wind speeds in the range of 15-20 m/sec.

The neural network results of SBB are reproducible for both the clear and cloudy cases using the same data for training and testing, and a network with the same architecture. In some cases, it was possible to improve upon the results of SBB using the NN1 and NN2 neural networks, although these improvements were small. These improvements, where they occurred, were most likely due to differences in the training

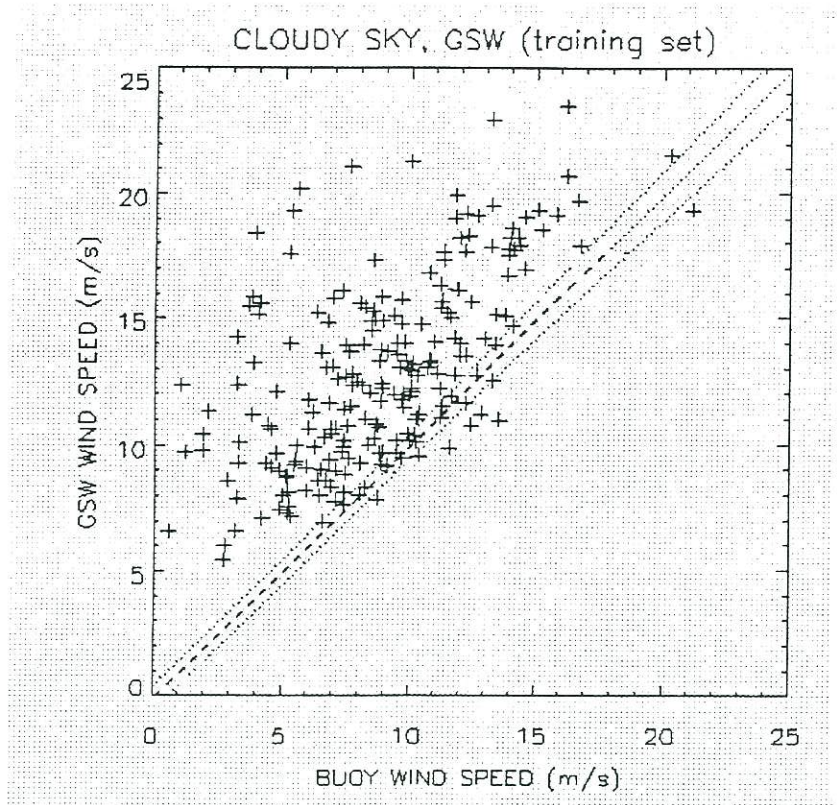

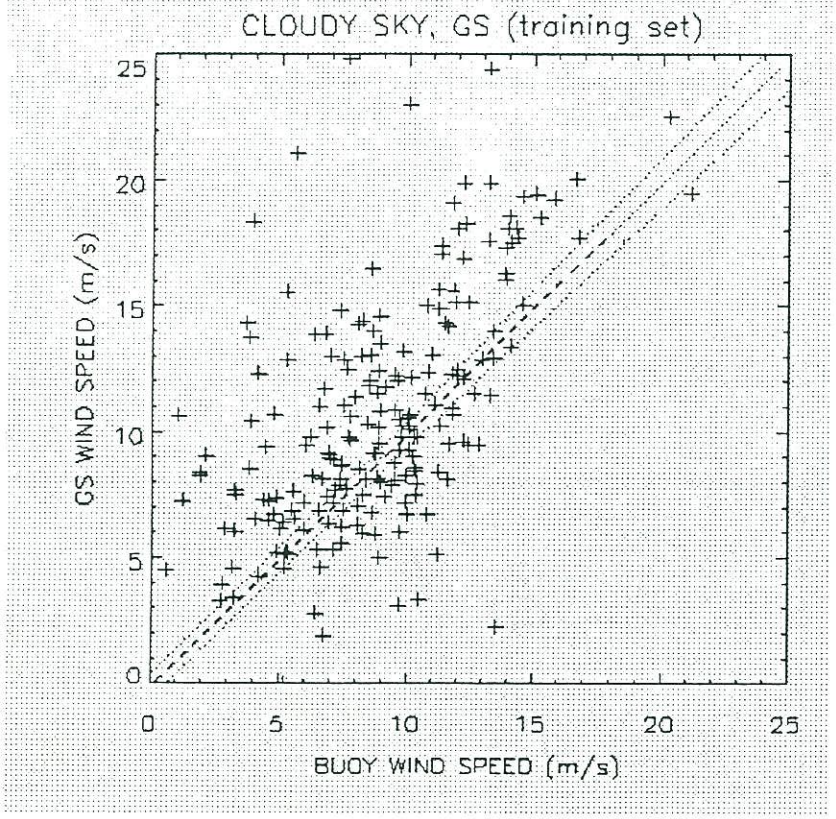

Fig. 10 (top) and Fig. 11 (bottom). Scatter plots for GSW and GS algorithms

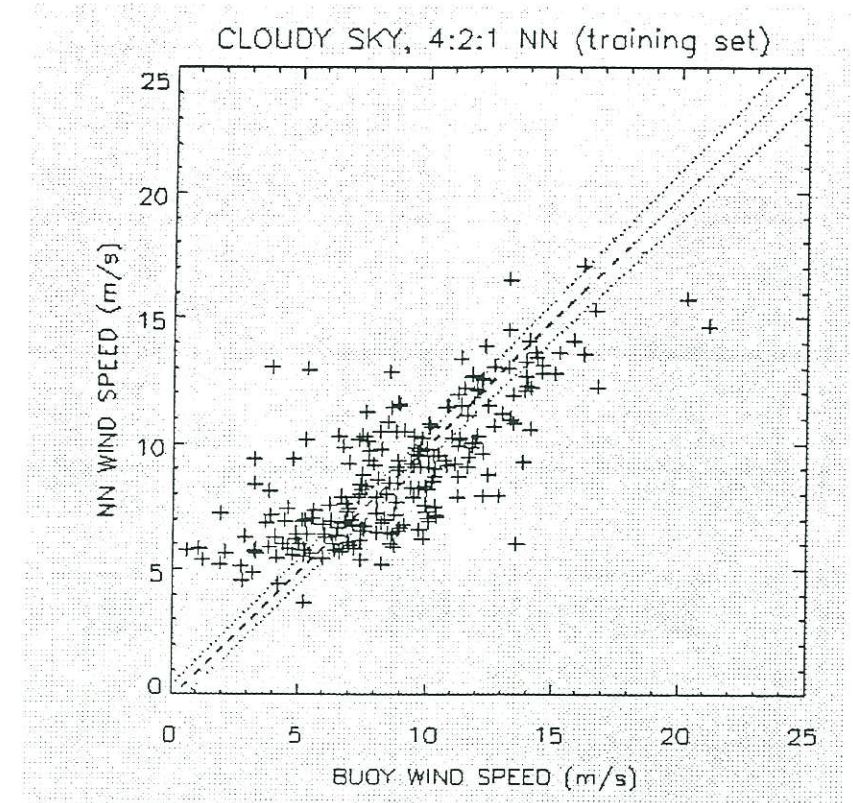

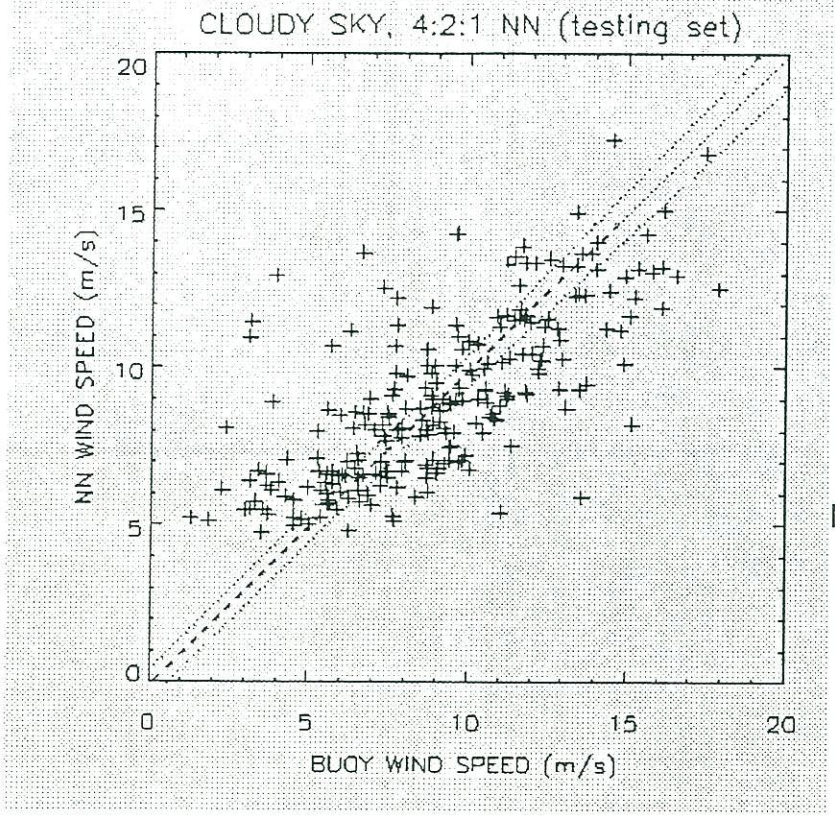

Fig. 12 (top) and Fig. 13 (bottom). Scatter plots for NN2 on the training and test sets.

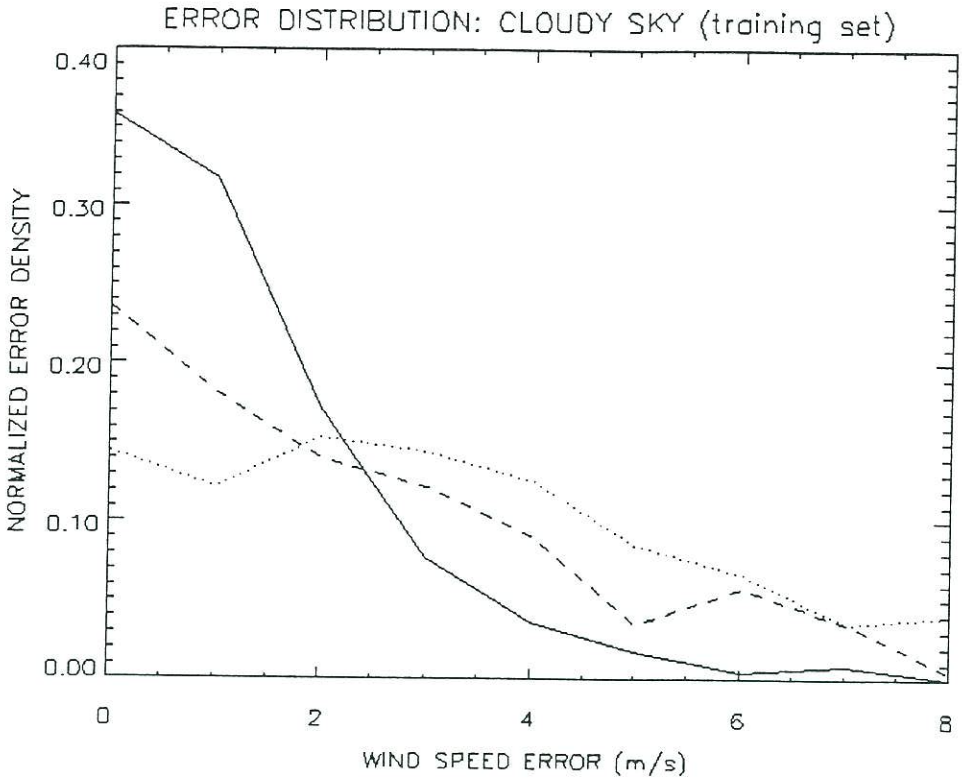

Fig. 14. Error distributions for NN2 (solid), GSW (dotted) and GS(dashed).

Table 8. Mean values and standard deviations for cloudy conditions (set # 2).

Source	Mean w	Mean w^2	σ
Training set			
Buoy data	8.89	91.7	3.57
GSW	12.9	179.6	3.69
GS	10.2	207.8	10.1
NN2	8.88	86.2	2.71
Test set			
Buoy data	6.46	93.1	3.08
GSW	7.52	181.4	3.73
GS	6.71	251.7	3.89
NN2	6.48	88.1	2.77

process since the architectures employed were identical. In an effort to make further improvements, additional nodes were added to the hidden layer (i.e., changing the NN architecture) but no improvement was found, consistent with the results of SBB. Also, the GSW algorithm output itself was used as an additional input to our NNs but again no improvement was found.

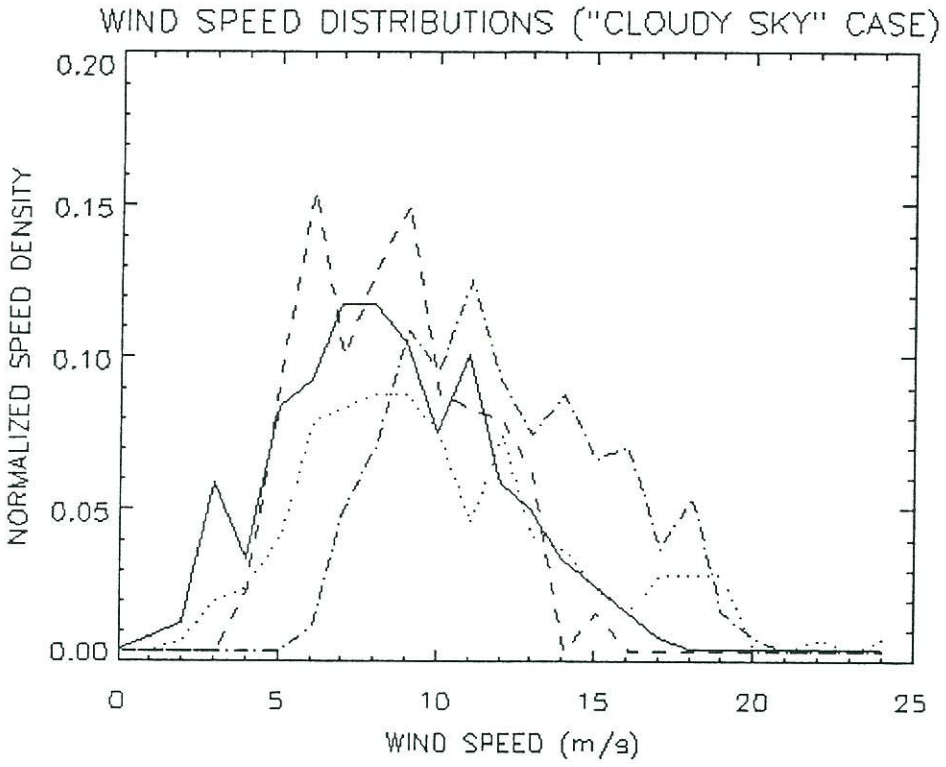

Fig. 15
Wind speed distributions for the cloudy case. Buoy winds (solid), NN (dashed), GSW (dotted) and GS (dot-dashed) - produced winds.

The weights that were obtained for the NN1 and NN2 neural networks for the clear and cloudy cases were quite different from those obtained by SBB. This result is due to the fact that NNs are inherently nonlinear (due to the nonlinear "squashing" functions employed) and during the training process, as convergence takes place, there is no quarantee it will lead to the same set of weights (i.e., the same local minima in the error

function (15)) in each case. The local minima which are found depend strongly on the weights that are chosen initially in the training process and, as mentioned earlier, they are often selected randomly (as was done by SBB) or, in some cases, using other approaches (as was done here).

7. DEVELOPING AN IMPROVED NEURAL NETWORK WIND SPEED RETRIEVAL ALGORITHM

a. Additional SSM/I channels

As a first step in exploring ways of improving SSM/I wind speed retrievals using NNs, we revisited the question of SSM/I channel selection. The results of GSW and SBB indicated that only four channels (i.e., 19.3 GHz(V), 22.2 GHz(V), 37 GHz(V), and 37 GHz(H)) of the SSM/I are required and that including additional channels yields no improvement in wind speed retrieval accuracy. Our results confirm their conclusions for clear conditions when additional channel inputs were included in the training process. However, this is not the case for cloudy conditions. For cloudy conditions, we trained and tested NNs with a 5th input. In the first case, we included the 19.3 GHz(H) channel, in the second case, the 85.5 GHz(V) channel, and in the third case, the 85.5 GHz(H) channel. The results are summarized in Table 9. Inclusion of the 19 GHz(H) channel provides little or no improvement. However, inclusion of the 85.5 GHz(V) and 85.5 GHz(H) channels indicate small but noticeable improvements. In Table 9 we call the NN with 5 inputs, NN3 (T19H, T85H or T85V as the 5th input). When both 85 GHz channels are included (i.e., with 6 NN inputs), no further improvement occurs for the training set and only a slight improvement for the test set (NN4 in Table 9). Because the sample sizes are relatively small for the cloudy case (~ 300 matchups in each case), these results must be considered preliminary. Thus, our results agree with SBB for clear conditions, but not for the cloudy case, although consistent with their findings, we find no improvement in either case by including the 19.3GHz channel.

Table 9. Performance of different NNs with a fifth input on the training and test sets for cloudy conditions (set # 2).

Algorithm	Bias	RMS	Corr. Coeff.	Skewness
Training set				
NN3 (T19H)	0.007	2.27	0.772	-0.557
NN3 (T85V)	0.09	2.19	0.789	-0.382
NN3 (T85H)	0.003	2.17	0.793	-0.363
NN4(T85H,V)	-0.002	2.23	0.779	0.029
NN2(4 inputs)	0.006	2.30	0.765	-0.496
Test set				
NN3 (T19H)	0.05	2.38	0.713	-0.608
NN3 (T85V)	0.07	2.14	0.776	-0.459
NN3 (T85H)	0.09	2.10	0.785	-0.461
NN4(T85H,V)	0.22	2.06	0.799	-0.017
NN2(4 inputs)	0.02	2.38	0.711	-0.578

b. Combined clear and cloudy conditions

As mentioned earlier, SBB employed separate NNs for the clear and cloudy cases. This piecewise approach implies that the differences in moisture were such that one NN could not be trained to cover the entire range of atmospheric conditions encountered. This piecewise approximation also produces a discontinuity in the region that separates the clear and cloudy cases according to the definitions employed by SBB. Due to the flexibility of NNs (because they can be trained to represent complicated nonlinear input/output relationships), we proceeded to combine the clear and cloudy matchups (subsets #4 = #1 + #2) to produce data that cover a wider (and continuous) range of atmospheric conditions in an effort to represent these composite data by **a single NN**.

Table 10 shows the performance of a single NN (NN5 with 4 inputs) trained on the combined clear and cloudy matchups for data set #4. Because the high wind

speed/high moisture cases are so underrepresented in this sample, we have simply retained the 4:2:1 architecture in the following results. Table 10 shows a comparison of NN5 with GS for the combined data. NN5 was also applied to the clear (#1) and cloudy (#2) subsets for further comparisons.

Table 10. Statistics for different NNs on the training and test set and their subsets for combined clear and cloudy conditions.

Data set	# 4		# 1		# 2	
Algorithm	GS	NN5	NN5	NN1	NN5	NN2
Training set						
Bias	-0.312	0.001	0.008	0.001	-0.054	0.006
RMS	3.81	1.54	1.39	1.38	2.40	2.30
Corr.Ceff.	0.652	0.874	0.887	0.888	0.741	0.765
Skewness	9.787	-0.290	-0.167	-0.219	-0.368	-0.496
Test set						
Bias	0.469	-0.027	-0.027	-0.02	-0.026	0.02
RMS	35.6	1.56	1.41	1.40	2.37	2.38
Corr.Ceff.	0.069	0.876	0.889	0.891	0.721	0.711
Skewness	41.85	-0.266	0.029	0.073	-0.653	-0.587

Application of NN5 to both the clear and cloudy cases show results almost identical to those obtained earlier using the previous algorithms (NN1 and NN2) which were trained separately for the low and higher moisture/higher wind speed subsets. When this single algorithm is applied to the combined data sets, we obtain results which are more-or-less mid-way between the results obtained for the two separate cases (excluding the biases). Also, the biases are less than 0.1 m/sec in all cases.

These results indicate that **a single NN** can be trained to perform as well on the combined clear and cloudy data sets as **separate NNs** trained on the clear and cloudy cases on an individual basis. By using a single NN we have also removed

any discontinuities in the SSM/I wind speeds in the region that separated the clear and cloudy cases as previously defined by SBB.

c. "All-weather" case

Because of the importance of being able to retrieve surface wind speeds under adverse weather conditions operationally where the levels of atmospheric moisture may be high, we examined the data previously labelled very cloudy (subset #3) to determine if a NN could be trained to work effectively in this region and to produce a contnuous wind speed field without gaps. As indicated, subset #3 is characterized by the presence of clouds, rain, or high humidity, and so our expectation was that the surface wind speed signal would most likely be undetectable. In order to conduct NN training, the entire training and test data sets were used. The results of the network (NN6 or "all-weather") trained on the entire data sets (#5 = #1 + #2 + #3) together with the results of applying this network to the previous clear (#1) and cloudy (#2) subsets separately (along with the previous "clear" (NN1) and "cloudy" (NN2) NN results) are presented in Table 11. Results using the GS algorithm are indicated for comparison. First, we note that NN6 produces results which are similar to the "clear" and "cloudy" NNs (NN1 and NN2) when applied to the previous clear and cloudy data sets separately. Second, and most surprising, is that when NN6 was tested on the entire data sets, the biases remained small (< 0.05 m/sec) and the rms differences increased only slightly (< 10%). This new result suggests that wind speed retrievals may in fact be possible under higher moisture/wind speed conditions than previously considered.

Figs.16-19 show scatter plots of SSM/I wind speed for the GSW, GS, and NN6 algorithms versus buoy wind speed for the entire test data set. In these figures, the line y = x indicates perfect agreement. These plots consistently show that the NN6 algorithm

Table 11. Statistics for the different NNs applied to the training and test sets and associated subsets (see text for details).

Data set	# 5		# 1		# 2	
NN #	GS	NN6	NN6	NN1	NN6	NN2
Training set						
Bias	-1.11	0.001	0.009	0.001	-0.054	0.006
RMS	13.5	1.64	1.40	1.38	2.40	2.30
Corr.Ceff.	0.25	0.858	0.885	0.888	0.741	0.765
Skewness	-26.74	-0.047	-0.120	-0.219	-0.368	-0.496
Test set						
Bias	0.492	-0.045	-0.035	-0.02	-0.024	0.02
RMS	39.4	1.65	1.42	1.40	2.38	2.38
Corr.Ceff.	0.073	0.863	0.887	0.891	0.744	0.711
Skewness	33.8	-0.165	0.080	0.073	-0.375	-0.587

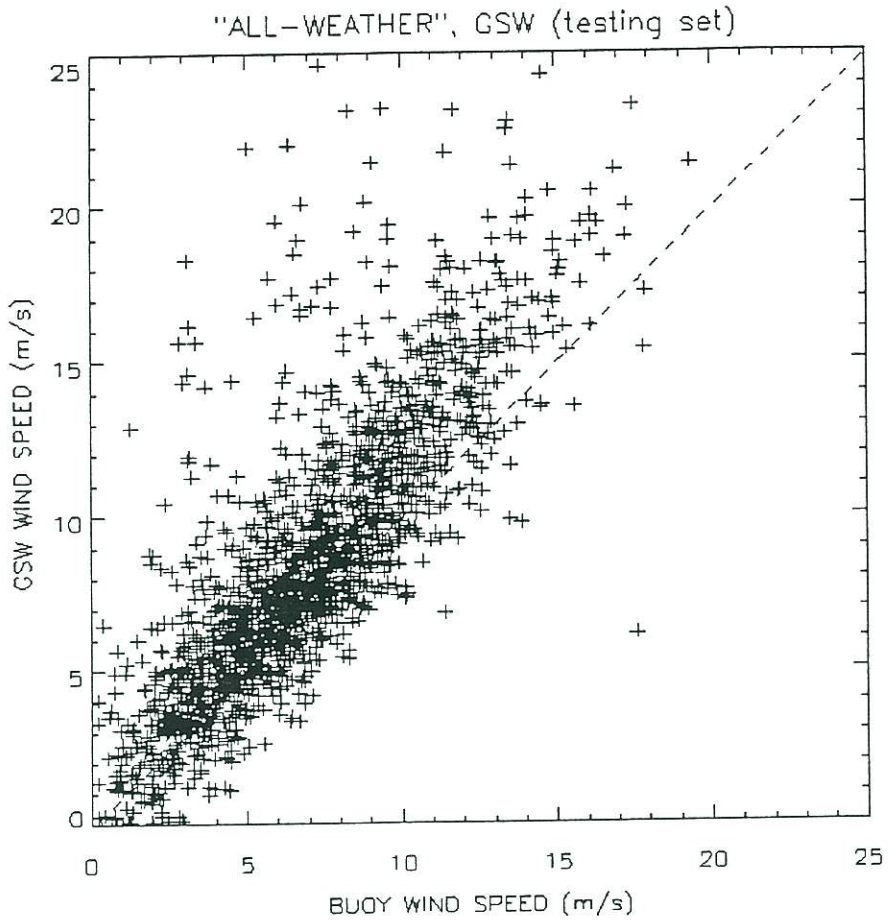

Fig. 16. Scatter plot for GSW algorithm

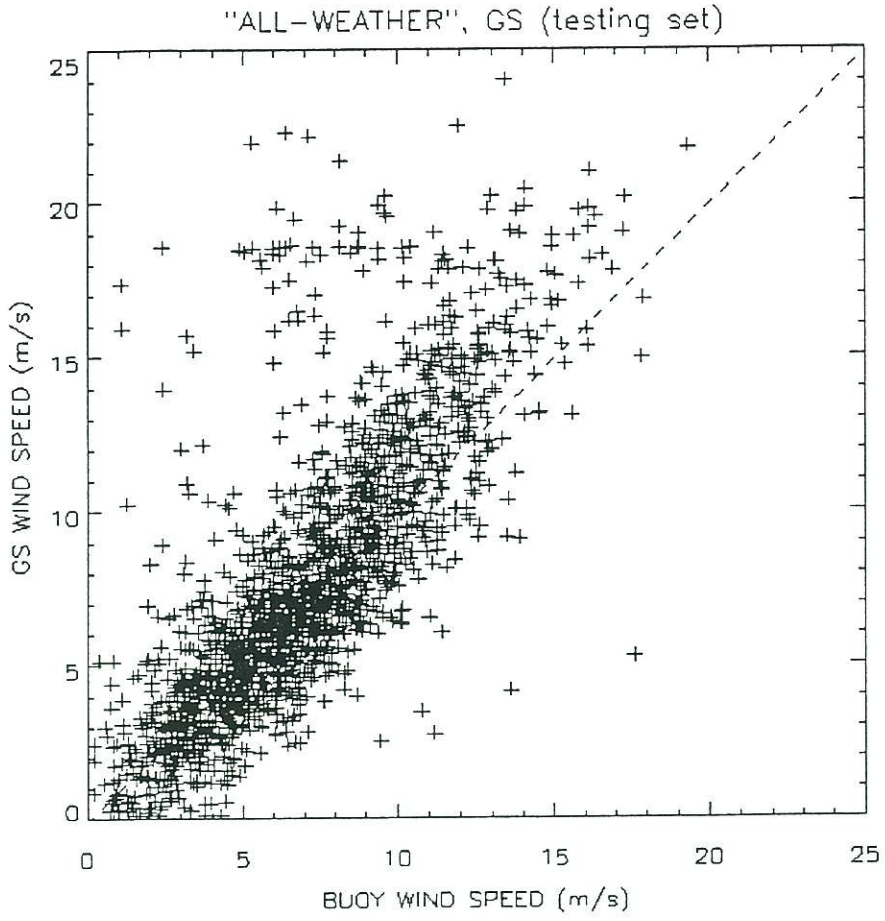

Fig. 17. Scatter plot for GS algorithm

produces less scatter and a better fit to the observed wind speeds than the other algorithms. Fig. 20 shows the error density distribution for wind speed for the NN6, the GSW, and the GS algorithms. NN6 produces a tighter fit to the ordinate and a smaller tail than the other algorithms, indicating better performance overall.

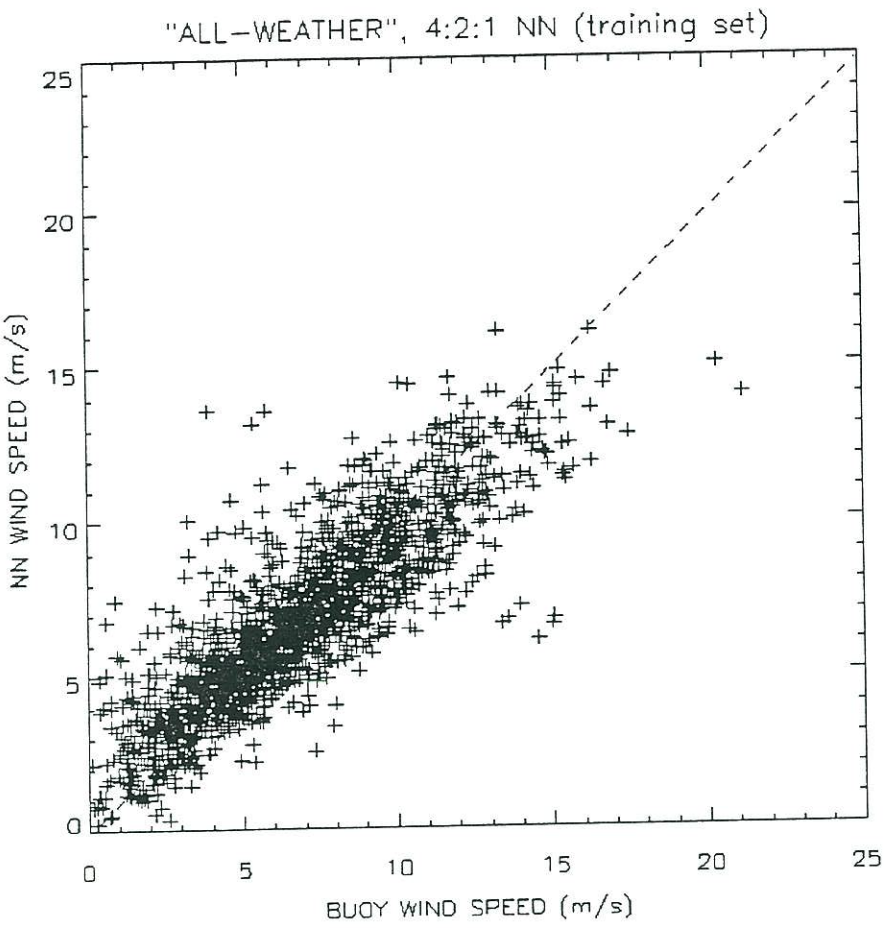

Fig. 18. Scatter plot for NN6 (training set)

Table 12 presents the means and standard deviations for the entire training and test data sets for the buoy observations and for the algorithms indicated. Note that the clear and cloudy NNs (NN1 and NN2) have been applied only to the clear and cloudy subsets. Of particular note is the close agreement between the observed means and standard deviations and those reproduced with NN6 for the entire data sets. Finally, wind speed distributions for the observed buoy data together with the algorithm-derived distributions for GSW and NN6 are shown in Fig. 21. NN6 reproduces the observations far better than GSW at wind speeds above 8 m/sec.

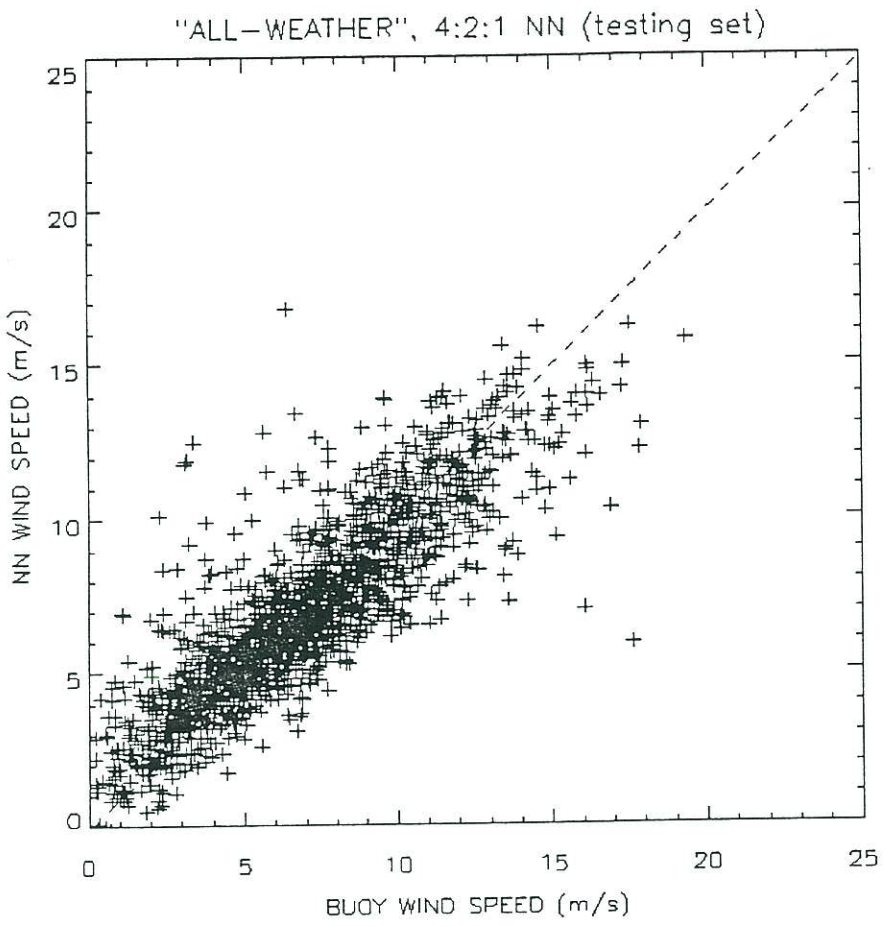

Fig. 19. Scatter plot for NN6 (test set)

Table 12. Means and variances for entire training and test data sets for the algorithms indicated.

Data sets	# 5			# 1			# 2		
NN #	Set	GS	NN6	Set	NN6	NN1	Set	NN6	NN2
Training set									
Mean	6.75	7.86	6.72	6.41	6.40	6.41	8.89	8.91	8.88
σ	3.19	13.9	2.73	3.01	2.62	2.67	3.57	2.73	2.71
Test set									
Mean	6.82	6.32	6.86	6.46	6.49	6.48	9.04	9.07	9.02
σ	3.25	39.5	2.85	3.08	2.75	2.77	3.39	2.64	2.61

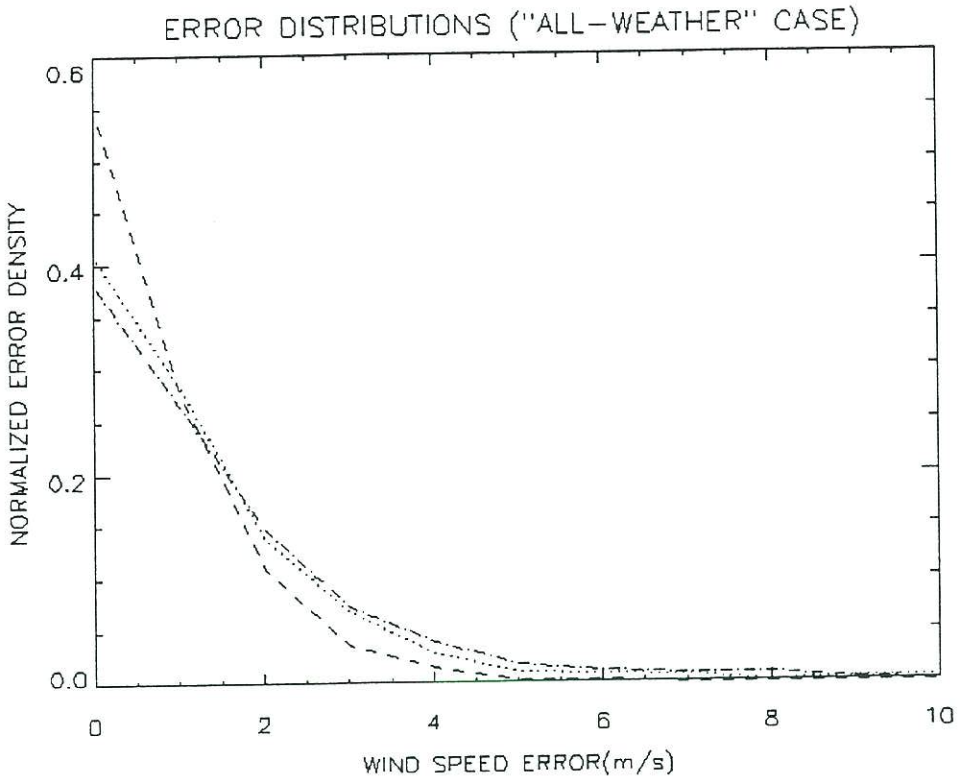

Fig. 20. Error distributions for NN6 (dashed), GSW (dotted) and GS(dot-dashed) algorithms

Table 13. Statistics for the various algorithms for the training and test data subsets #3 (very cloudy conditions).

	GSW	GS	NN1	NN2	NN5	NN6
Training set						
Bias	-29.6	-21.4	-6.2	-2.7	-3.0	-0.13
RMS	39.4	66.6	8.6	8.7	7.0	3.19
Test set						
Bias	-30.4	1.2	-7.3	-1.7	2.9	-0.34
RMS	37.6	98.6	9.5	7.4	6.6	3.2

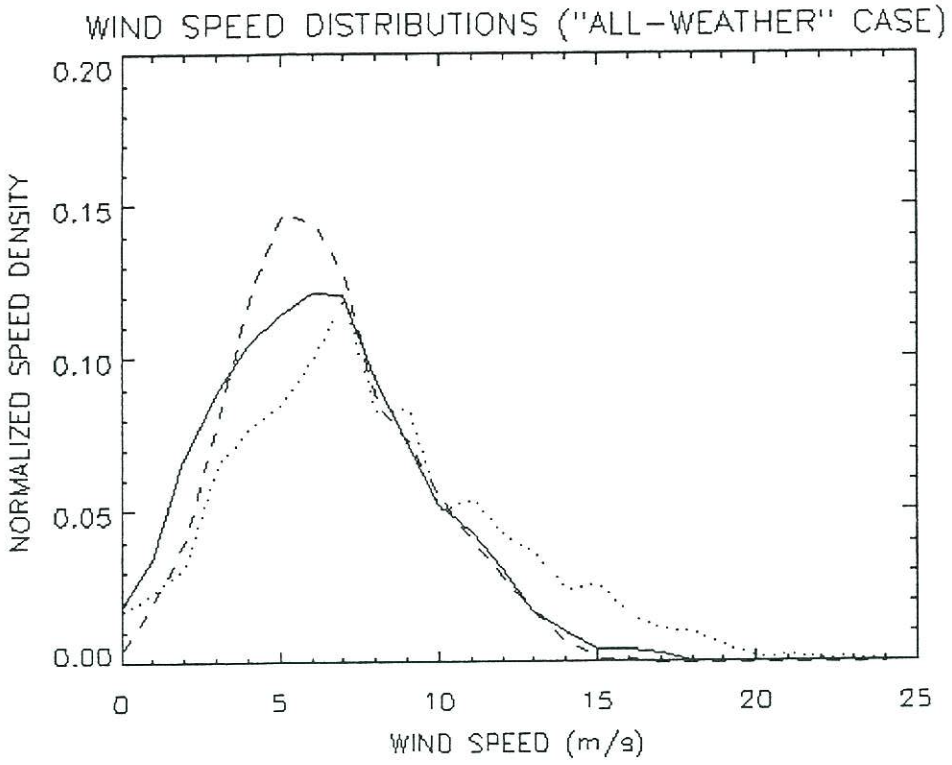

Fig. 21. Wind speed distributions for the "all-weather" case. Buoy winds (solid), NN (dashed), and GSW (dotted) produced winds.

To further explore the possibility of making wind speed retrievals under adverse weather/high moisture conditions, we go one step further and apply the NN6 algorithm (plus previous networks) separately to the very cloudy data subsets (#3) bearing in mind that these samples are extremely small (75 matchups in the training set and 68 matchups in the test set) and so any conclusions we draw at this point must be strictly tentative. To more fully interpret the results, it would be important to examine the synoptic conditions that prevailed for these various "very cloudy" matchups. From Table 13, only the NN6 algorithm produces results which might be considered acceptable, yielding biases of < 0.4 m/sec, and RMS values of 3.2 m/sec. These values are only slightly higher than the previous values and are consistent between the training and test data sets, suggesting that at least a weak signal from the ocean surface remains in the SSM/I TBs. Table 14 shows

how well the various algorithms reproduce the sample statistics, with NN6 again clearly coming out on top.

Table 14. Means and variances for training and test data subset #3 for the various algorithms indicated.

	Set	GSW	GS	NN1	NN2	NN5	NN6
Training set							
Mean	8.03	37.6	29.4	14.2	10.8	11.1	8.2
σ	3.19	25.4	63.5	4.8	7.3	5.1	1.7
Test set							
Mean	7.86	38.2	6.7	15.2	9.6	10.7	8.2
σ	3.55	21.1	99.6	4.4	6.4	4.7	1.7

Figs. 22 and 23 are scatter plots for the NN6 and the GSW-derived wind speeds versus buoy wind speed observations. As expected, the NN6-derived wind speeds match the observed wind speeds far better than GSW. We also note from Table 14 and Fig.24 that the actual wind speeds in this subset are all less than 17 m/sec, indicating the expected result that high moisture conditions do not necessarily imply high wind speeds. Fig. 24 further supports the improvement achieved using NN6 (vs. GSW) in reproducing the wind speed distribution for this subset.

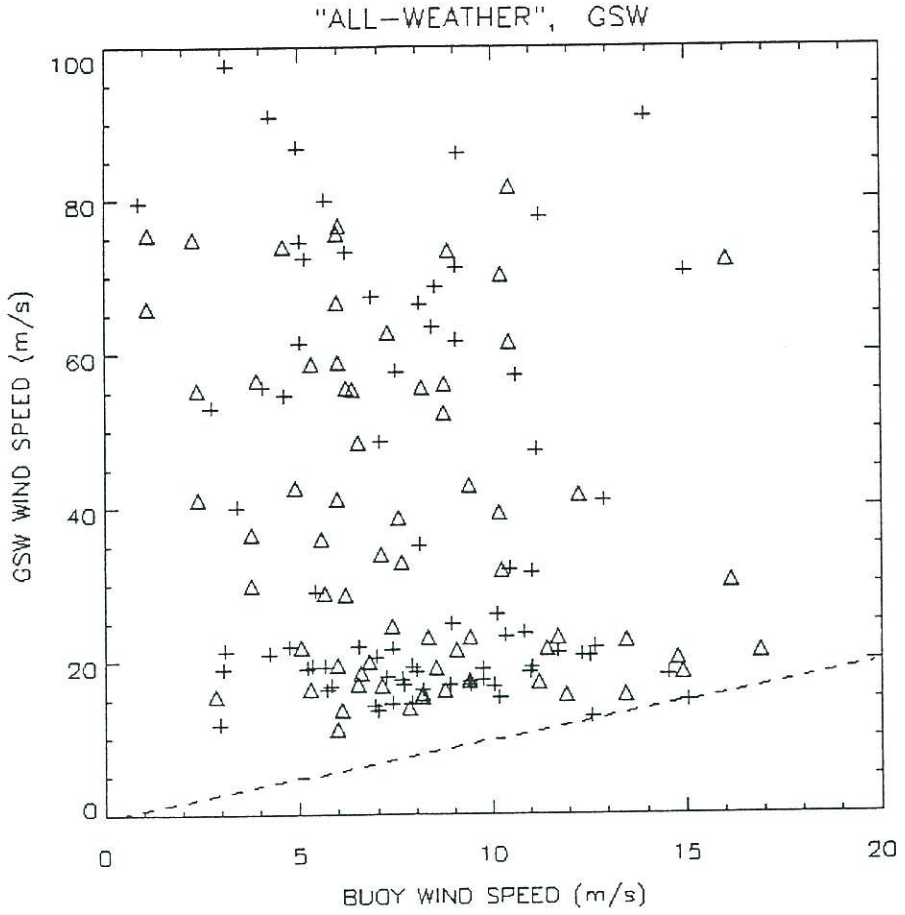

Fig. 22. Scatter plot for GSW algorithm for subset #3. Crosses are points from the training set and triangles are points from the test set.

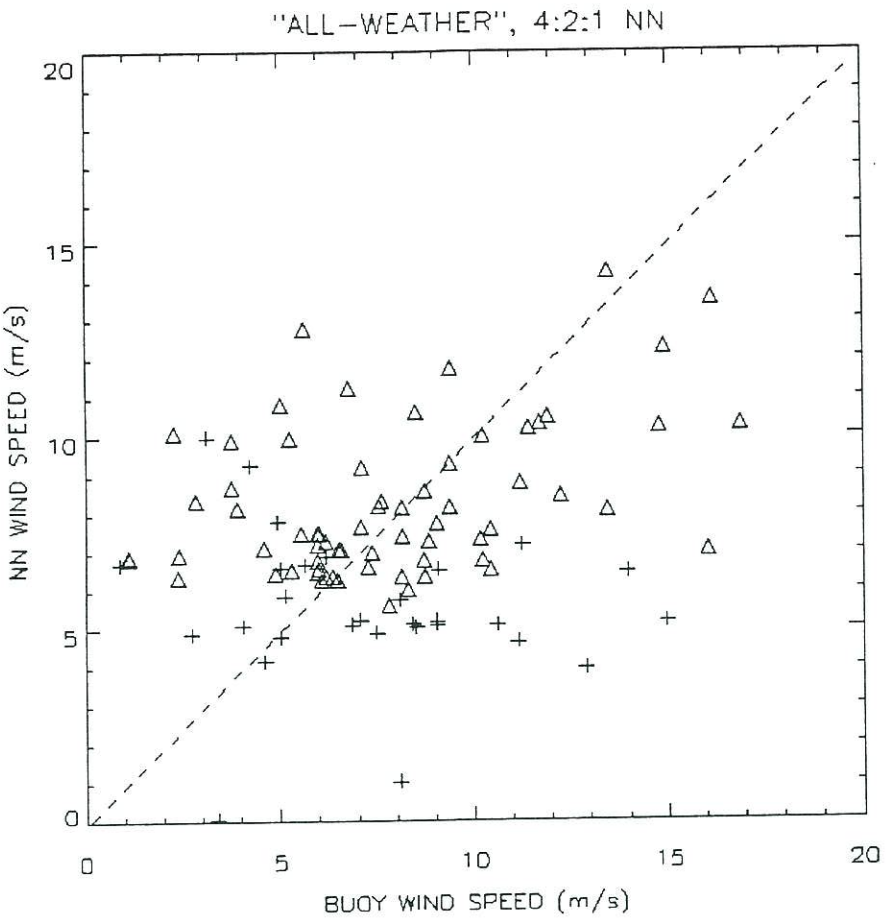

Fig. 23. Scatter plot for NN6 for subset #3. Crosses are points from the training set and triangles are points from the test set.

Only the standard four channels were used in deriving the results for the last case. Based on our earlier results, we did not expect much improvement in the performance of our "all-weather" NN when the additional 85 GHz(H) and 85 GHz(V) channels were included. To verify this result, we constructed and trained one more NN with 6 inputs (NN7). This network was trained on the entire training and test data sets. The results of applying both the 6 (NN7) and the 4-input (NN6) NNs to all of the previous data sets are shown in Table 15. From this table, NN7 only outperforms NN6 for the cloudy and very cloudy cases. However, it must be remembered that approximately 90% of the entire data sets (see Table 1)correspond to clear conditions and thus are

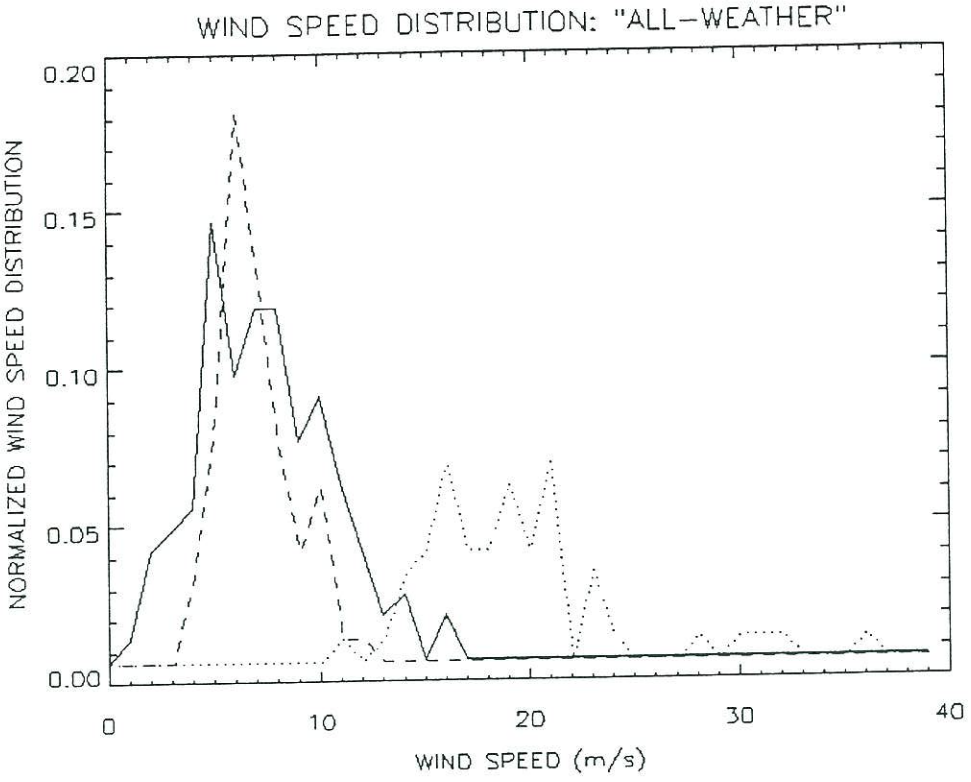

Fig. 24. Wind speed distributions for subset #3; buoy winds (solid), NN6 (dashed) and GSW (dotted) - produced winds.

disproportionately represented in this overall sample. This once again emphasizes the need for matchup data where all atmospheric conditions and wind speeds are more uniformly represented. With respect to the third subset, we have applied several TB discriminants to this sample to determine if we could establish a region beyond which retrievals were meaningless but below which useful retrievals might still be obtained. It is important to note that the only criteria we found applicable was the one given by SL, where 5K < (TB85V - TB37V) < 55K. When this discriminant was applied to the third subset, about 30% of the data were rejected.

Table 15. Statistics for various NNs for entire training and test sets and subsets.

Data set	# 5		# 1		# 2		# 3	
NN #	NN6	NN7	NN6	NN7	NN6	NN7	NN6	NN7
Training set								
Bias	0.001	0.001	0.009	0.011	-0.024	-0.065	-0.128	-0.071
RMS	1.64	1.64	1.40	1.42	2.38	2.32	3.19	3.11
Corr.Ceff.	0.858	0.858	0.885	0.881	0.744	0.760	0.257	0.239
Skewness	-0.047	-0.102	-0.120	-0.126	-0.375	-0.450	0.633	0.532
Test set								
Bias	-0.045	-0.053	-0.035	-0.04	-0.025	-0.063	-0.340	-0.332
RMS	1.65	1.62	1.42	1.42	2.32	2.20	3.20	3.08
Corr.Ceff.	0.885	0.867	0.887	0.887	0.730	0.759	0.435	0.498
Skewness	-0.120	-0.165	0.080	0.135	-0.569	-0.654	0.134	0.034

However, the matchups that remained revealed about the same scatter as before. Because rain was most likely present in some (or most) of these data, this result is not surprising in view of the large inrease in TB variability that rain produces.

The weights, biases, and scaling parameters for the "all-weather" neural network (NN6) are presented in Table 16 below.

Table 16. Coefficients for the "all-weather" neural network (NN6).

$\Omega_{1,1}$	$\Omega_{1,2}$	$\Omega_{2,1}$	$\Omega_{2,2}$	$\Omega_{3,1}$	$\Omega_{3,2}$	$\Omega_{4,1}$	$\Omega_{4,2}$
6.618-2	7.075-2	-2.031-2	-6.488-3	-1.109-1	-3.573-2	4.503-2	8.020-3
ω_1	ω_2	B_1	B_2	β	*a*	*b*	
9.272-1	-3.839-1	8.508	-7.223	-7.595-1	17.52	10.64	

8. OPERATIONAL RESULTS

The motivation for the work presented up to this point has been to develop an improved NN algorithm for retrieving surface wind speeds from SSM/I satellite data for operational use at NMC. In addition to improved retrieval accuracy, expanded coverage, particularly in areas where significant weather is occurring has been a primary objective. Based on the results which have been presented, NN6 has been implemented on the experimental basis at NMC to provide additional estimates of surface wind speed over the ocean. This algorithm has been run in parallel with the presently operational GSW algorithm for the past few months and has shown significant improvement. Because the samples which have been acquired are still relatively small, we do not include quantitative results at this time.

As an indication of the qualitative improvement that can be achieved using NN6 versus GSW, maps of surface wind speed applying each algorithm to the same data are shown (Figs. 25 and 26) together with the corresponding NMC surface analysis (Fig.27) for 6 May, 1994. The NMC surface analysis depicts a surface low pressure system centered at approximately 43° N, 66° W, with corespondingly higher surface winds in the surrounding regions. Wind speeds as high as 45 knots are reported at 43° N, 60.5°W, but the other reports tend to be in the range of 20-30 knots. Due to the TB restrictions for GSW, the region of higher winds and moisture that surround the surface low are excluded from consideration. However, no similar restrictions have been applied to NN6 and, as a result, the gap that arises in using GSW is completely filled when NN6 is applied. Although the NN6-produced wind speeds are somewhat lower than the model-produced wind speeds in the area surrounding the low, they do show slightly higher winds in the area of low pressure indicated in the NMC analysis.

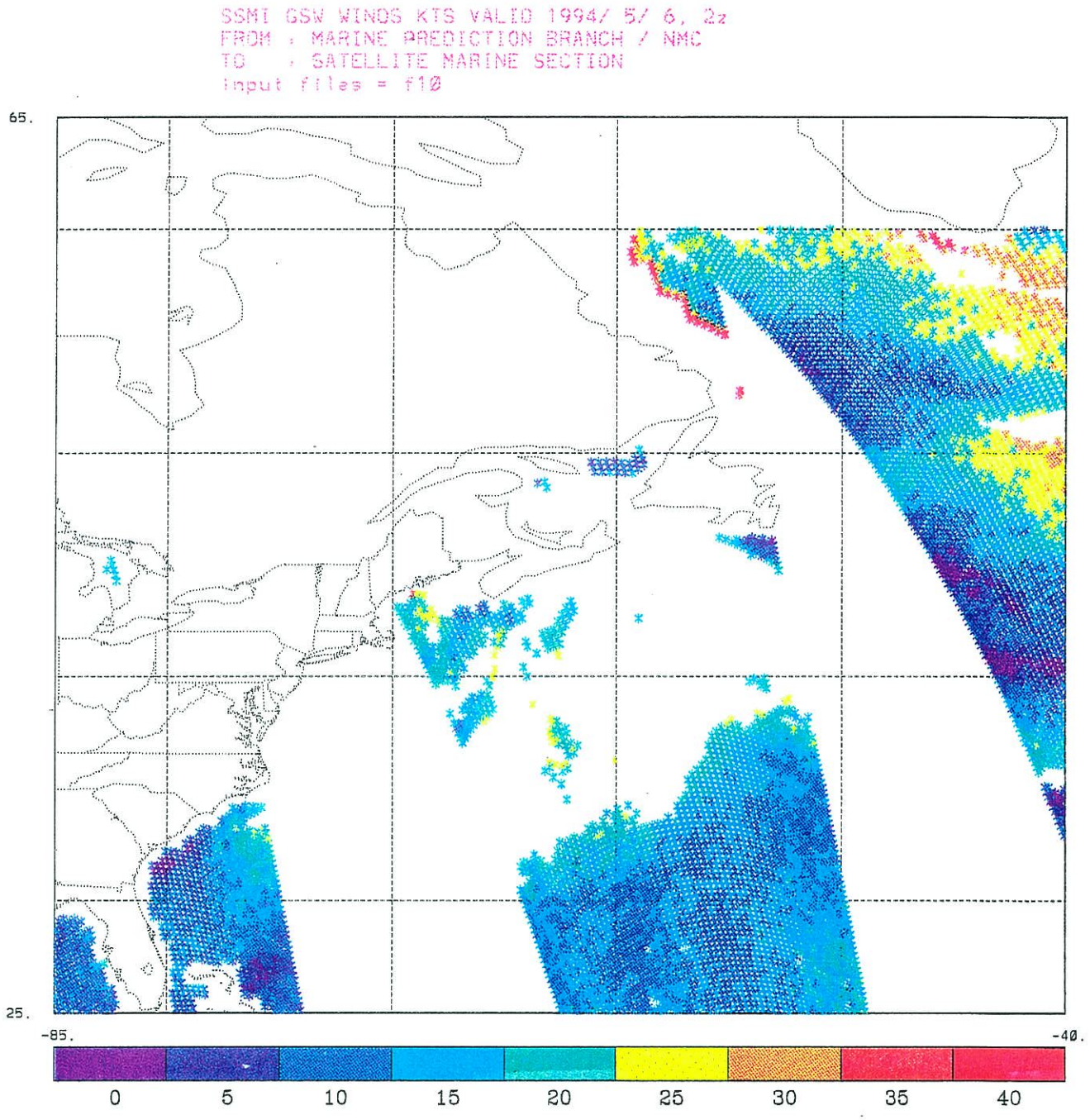

Fig. 25. GSW map of surface wind speed for May 6, 1994.

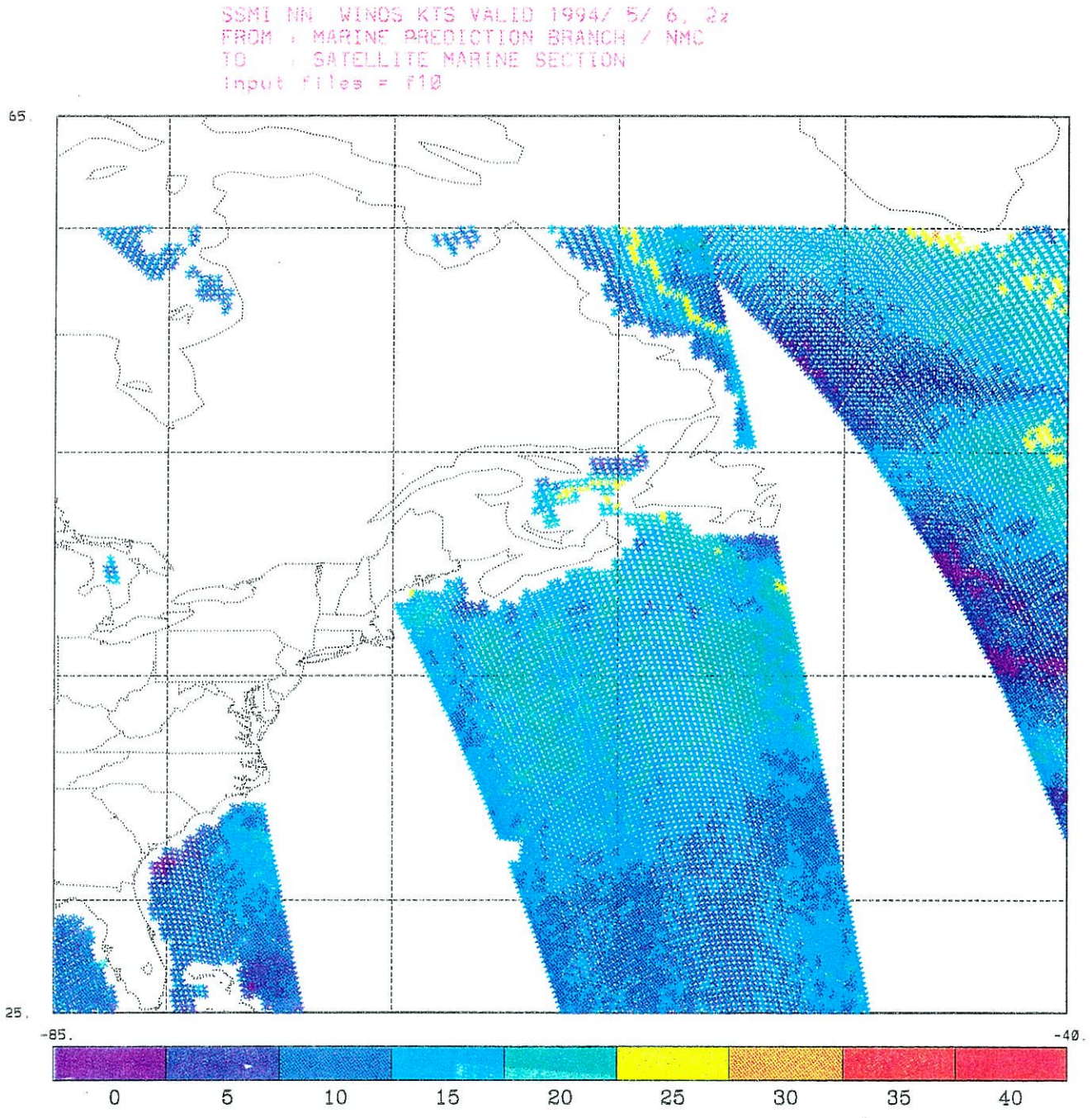

Fig. 26. NN map of surface wind speed for May 6, 1994.

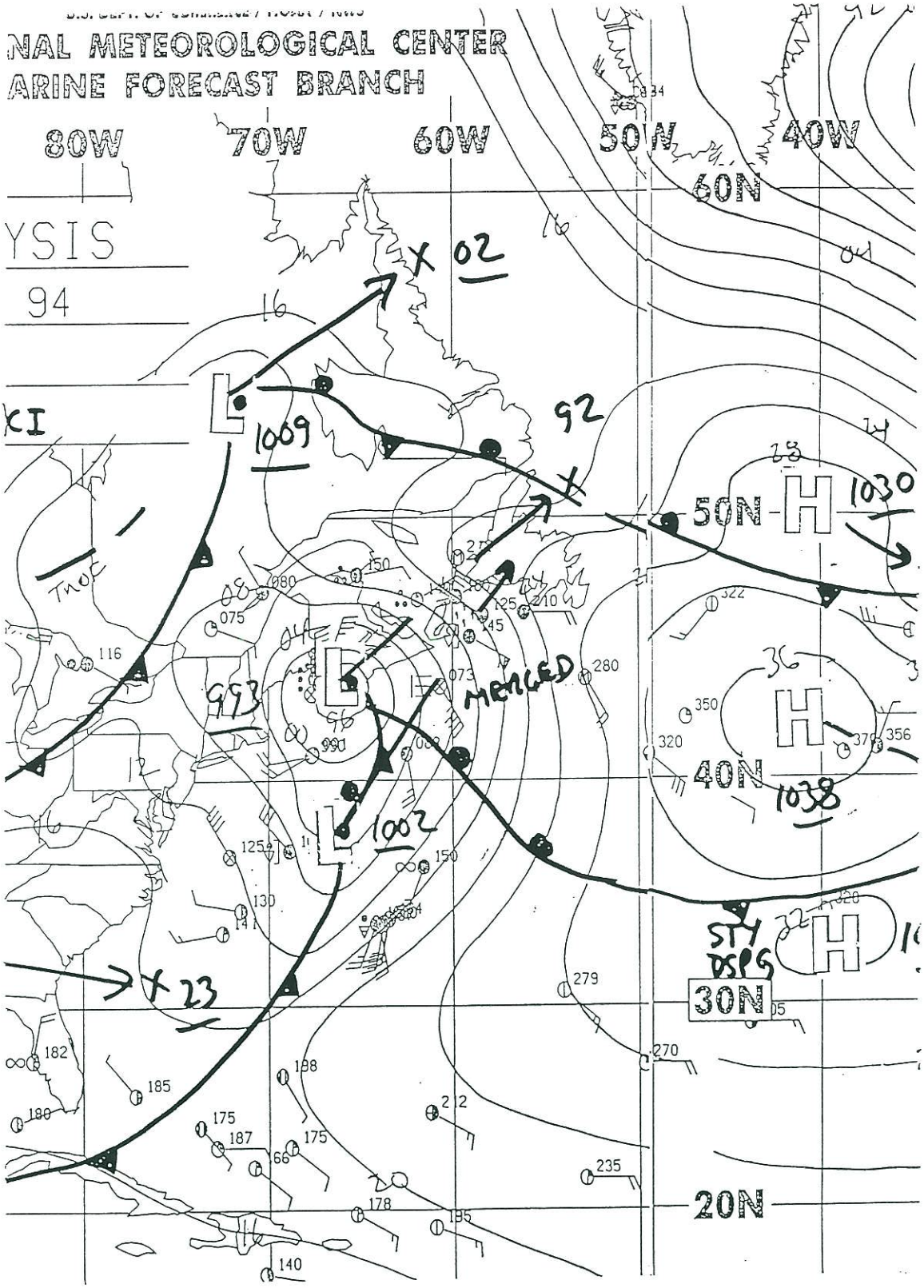

Fig. 27. NMC surface analysis for May 6, 1994.

As better training sets become available, it will be a relatively simple matter to retrain NN6 to yield better wind speed estimates under higher wind speed conditions. Also, although no rain flag criteria were applied to these data using NN6, it is our expectation that rain flag criteria will most likely be required under very adverse atmospheric conditions. As more experience is gained in applying this algorithm to high moisture/high wind speed situations, we should be able to arrive at appropriate TB discriminants.

9. DISCUSSION AND CONCLUSIONS

Most of the work that has been accomplished in developing wind speed retrieval algorithms for SSM/I satellite data has focussed primarily on low moisture/low wind speed conditions. Clearly, the wind speed signal from the ocean surface is much easier to identify and retrieve in these cases. Operationally, it is also important to be able to retrieve surface wind speeds under adverse atmospheric conditions as well. For example, it is important to acquire surface winds associated with oceanic low pressure systems and in the vicinity of fronts. Unfortunately, these synoptic-scale and mesoscale features are often accompanied by clouds and rain.

In support of the above, it should be possible to derive better rain flag criteria for high moisture situations by giving closer attention to the moisture conditions that prevail in each case. It is reasonable to expect that the rain flag criteria which apply for light rain at mid-latitudes may be quite different from the rain flag criteria that apply for high humidity conditions in the tropics. Similarly, the appropriate rain flag criteria for deep convective activity and heavy cumulus will most likely be quite different from either of the above.

The results presented earlier plus the work of others (e.g., Black and Swift, 1984) suggest that a detectable wind speed signal may, in some cases, exist under very adverse atmospheric conditions. Based on the aircraft measurements of Black and Swift (1984) it may be possible to measure wind speeds up to 70 m/sec. To confirm these results and to make further improvements to the algorithm presented here, a new SSM/I/wind speed matchup database is needed which places greater emphasis on high moisture/high wind speed conditions.

NNs have produced better results than those obtained using conventional fitting techniques for several reasons. First, NNs are essentially nonlinear because they contain a nonlinear (squashing) function in each processing element. Thus, NNs are able to reproduce input/output relationships which are inherently nonlinear. Also, no specific analytic representation for such nonlinear relationships must be assumed in constructing the network; therefore, NNs can be used as general nonlinear transfer functions. They

should also perform satisfactorily when the functional form of the input/output relationship changes over the dynamic range of the measurements. This may be particularly important for the SSM/I TB/wind speed relationship (Swift, 1990). Second, NNs have been shown to work well in low signal-to-noise environments (Kerlirzin and Vallet, 1993; Feng and Schulteis, 1993). This characteristic may be important in the present application when rain and/or other forms of atmospheric moisture are present.

One of the characteristics of the NNs presented here is that they consistently produced lower measures of variability than that actually contained in the observations themselves, a characteristic shared by regression models as well. Although this behaviour may be characteristic of NNs, it should be possible to modify the error or cost function in such a way that this variability is not suppressed but rather is amplified according to the manner in which the cost function is parameterized.

In the future, there are additional steps that can be taken to further improve surface wind speed retrievals from the SSM/I. First, errors in the buoy observations themselves should be taken into account. Also, improvements can be made to the way in which the SSM/I/buoy wind speed matchups are produced. For example, weights can be assigned to the surrounding SSM/I data that depend on the distance between the SSM/I reports and the buoy.

It may be possible to improve SSM/I wind speed retrieval accuracy by using the raw radiances from the SSM/I versus the microwave TBs which are now used. This improvement in accuracy would occur through the elimination of the intermediate step of calculating brightness temperatures.

It was shown that a slight improvement in NN retrieval accuracy could be achieved by including the 85 GHz H or V channel inputs. This improvement, however, occured only for the cloudy and very cloudy cases. This improvement is most likely due to the higher spatial resolution of the SSM/I at 85 GHz (12.5 km vs. 25 km at the lower frequencies) which should help significantly in resolving fine scale patterns of rain and moisture when and where they occur.

Finally, based on the work of Wentz (1992), it may be possible to estimate wind direction as well as wind speed from SSM/I data. Because the relationship between TB and wind direction is undoubtedly complicated, NNs may again be well-suited to the task of establishing this relationship. In this regard, we note that Thiria et al. (1991) have successfully applied NNs to the wind direction (and speed) retrieval problem for scatterometer data acquired from the ERS-1 scatterometer.

We have reproduced the results of Stogryn et al. using the same SSM/I/buoy wind speed matchups and the same NN architecture. In some cases, even slightly better results were obtained which we attribute to differences in the NN training process. The NN yielded significantly better accuracy in retrieving surface wind speeds from the SSM/I than can be achieved using the currently operational algorithm of GSW (30% improvement under clear conditions and ~250% improvement under cloudy conditions).

We have extended the technique, developing a single "all-weather" NN which was applied over the entire range of weather conditions available in the matchup database. This NN produced continuous wind speeds without gaps over the entire range of wind speeds encountered. The accuracy of the "all-weather" NN for the clear and cloudy cases equals the accuracy of the separate NNs of Stogryn et al. (1994) for these specific conditions. Rain flag criteria will most likely be required under certain atmospheric conditions but they have yet to be determined.

We have shown that the NN algorithm presented here, in addition to producing a small bias and relatively small rms errors, reproduces the mean, standard deviation, and distribution of the observed sample wind speeds better than any of the other algorithms that were considered.

These results indicate that it may be possible to obtain SSM/I wind speed retrievals under more adverse atmospheric conditions than were previously considered using NNs as a basis. However, it will be important to (i) first create an SSM/I/buoy wind speed matchup database with a far greater number of matchups under high wind speed/high moisture conditions, and (ii), establish the range of atmospheric conditions (through the

appropriate TB discriminants) over which this extended algorithm will provide operationally useful results.

ACKNOWLEDGMENTS

We thank D.B. Rao for providing the encouragement needed to complete this study. We also thank Gene Poe from the Naval Research Laboratory for providing the SSM/I brightness temperature - buoy wind speed matchup data base.

REFERENCES

Alishouse, J.C., et al., "Determination of oceanic total precipitable water from the SSM/I", IEEE Transactions on Geoscience and Remote Sensing, **23**, 811-816, 1990

Black,P.G., and C.T.Swift, "Airborne stepped frequency microwave radiometer measurements of rainfall rate and surface wind speed in hurricanes", Proc. 22nd Conf. on Radar Meteor., AMS Publication, 433-438, 1984.

Gilhousen, D.B., "An accuracy statement for meteorological measurements obtained from NDBC moored buoys", paper presented at Marine Data Systems International Symposium, Mar. Technol. Soc., New Orleans, La.,1986.

Goodberlet M.A. et al., "Remote Sensing of Ocean Surface Winds with the Special Sensor Microwave/Imager", J. Geophys. Res., **94**, 14 574-14 555, 1989.

Goodberlet M.A. and C.T. Swift. "Improved retrievals from the DMSP wind speed algorithm under adverse weather conditions." IEEE Transact. Geophys. Sci. and Remote Sens., **30**, 1076-1077, 1992.

Feng X. and J. Y. Schulteis. "Idintification of High Noise Time Series Signals Using Hybrid ARMA Modeling and Neural Network Approach." in Proceedings of 1993 IEEE International Conference on Neural Networks, San Francisco, California, March 28 - April 1, 1993, ICNN, 1993, 1780 - 1785, 1993

Hollinger,J.P.,J.L.Peirce, and G.A.Poe, "SSM/I instrument evaluation", IEEE Trans. Geosci. Remote Sens.,GE-28, 781-790, 1990.

Kerlirzin P. and F. Vallet. "Robustness in Multilayer Perceptrons." Neural Computation, **5**: 473 - 482, 1993.

Lo,R.C., "A comprehensive description of the mission sensor microwave imager SSM/I environmental parameter extraction algorithm", NRL Memo. Rep., 5199, 1983.

Nguyen, D. and B. Widrow. "Improving the learning speed of 2-layer neural networks by choosing initial values of the adaptive weights." International Joint Conference of Neural Networks, July 1990, **3**, 21-26, 1990

Ostle B. and R.W. Mensing, Statistics in Research. Basis Concepts and Techniques for Research Workers. The Iowa State University Press, Third Edition, Ames, Iowa, 1975

Schluessel, P., and H. Luthardt, Surface wind speeds over the North Sea from special sensor micrwave imager observations, J. Geophys. Res., **96**, 4845-4853, 1991.

Simpson, P.K., Artificial Neural Systems, Pergamon Press, New York, 1990

Stogryn, A., The emissivity of sea foam at microwave frequencies, J. Geophys. Res., **77**, 1650-1666, 1972

Stogryn A.P., C.T. Butler, and T.J. Bartolac. "Ocean surface wind retrievals from special sensor microwave imager data with neural networks" J. of Geophys. Res., **90**, 981-984, 1994.

Swift, C.T., Passive microwave remote sensing of ocean surface wind speed,in Surface Waves and Fluxes, edited by G.L.Geernaert and W.L.Plant, 265-292, Kluwer Academic Publishers, Dordrecht, 1990.

Thiria, S., C. Mejia, F. Badran, and M. Crepon. A Neural Network Approach for Modeling non Linear Transfer Functions: Application for Wind Retrieval from Spaceborn Scatterometer Data. Preprint., LODYS, Paris, 1991

Ulaby, F.T.,r.T.Moore, and A.K.Fung, Microwave Remote Sensing Active and Passive,Vol. 3, Artech House, Norwood, MA, 1986.

Wasserman, P. D., Neural Computing,Van Nostrand Reinhold, New York, 1989.

Wentz, F.J., Measurement of oceanic wind vector using satellite microwave radiometers, IEEE Trans. Geosci. Remote sens., GE-30, 960-972, 1992.

Wentz F.J., L.A. Mattox, and S. Peteherych, "New algorithms for microwave measurements of ocean winds: applications tp SEASAT and the Spectral Sensor Microwave Imager", J. Geophys. Res., **91,** 2289-2307, 1986

Wessels L. F. A. and E. Bernard. "Avoiding False Local Minima by Proper Initialization of Connections." IEEE Transactions on Neural Networks , **3**: 899-905, 1992

No. 22. Yu, T.W., D.C. Esteva, and R.L. Teboulle, 1991: A Feasibility Study on Operational Use of Geosat Wind and Wave Data at the National Meteorological Center. Technical Note/NMC Office Note No. 380, 28pp.

No. 23. Burroughs, L. D., 1989: Open Ocean Fog and Visibility Forecasting Guidance System. Technical Note/NMC Office Note No. 348, 18pp.

No. 24. Gerald, V. M., 1987: Synoptic Surface Marine Data Monitoring. Technical Note/NMC Office Note No. 335, 10pp.

No. 25. Breaker, L. C., 1989: Estimating and Removing Sensor Induced Correlation form AVHRR Data. Journal of Geophysical Reseach, 95, 9701-9711.

No. 26. Chen, H. S., 1990: Infinite Elements for Water Wave Radiation and Scattering. International Journal for Numerical Methods in Fluids, 11, 555-569.

No. 27. Gemmill, W.H., T.W. Yu, and D.M. Feit, 1988: A Statistical Comparison of Methods for Determining Ocean Surface Winds. Journal of Weather and Forecasting. 3, 153-160.

No. 28. Rao. D. B., 1989: A Review of the Program of the Ocean Products Center. Weather and Forecasting. 4, 427-443.

No. 29. Chen, H. S., 1989: Infinite Elements for Combined Diffration and Refraction . Conference Preprint, Seventh International Conference on Finite Element Methods Flow Problems, Huntsville, Alabama, 6pp.

No. 30. Chao, Y. Y., 1989: An Operational Spectral Wave Forecasting Model for the Gulf of Mexico. Proceedings of 2nd International Workshop on Wave Forecasting and Hindcasting, 240-247.

No. 31. Esteva, D.C., 1989: Improving Global Wave Forecasting Incorporating Altimeter Data. Proceedings of 2nd International Workshop on Wave Hindcasting and Forecasting,Vancouver, B.C., April 25-28, 1989, 378-384.

No. 32. Richardson, W. S., J. M. Nault, D. M. Feit, 1989: Computer-Worded Marine Forecasts. Preprint, 6th Symp. on Coastal Ocean Management Coastal Zone 89, 4075-4084.

No. 33. Chao, Y. Y., T. L. Bertucci, 1989: A Columbia River Entrance Wave Forecasting Program Developed at the Ocean Products Center. Techical Note/NMC Office Note 361.

No. 34. Burroughs, L. D., 1989: Forecasting Open Ocean Fog and Visibility. Preprint, 11th Conference on Probability and Statisitcs, Monterey, Ca., 5pp.

No. 35. Rao, D. B., 1990: Local and Regional Scale Wave Models. Proceeding (CMM/WMO) Technical Conference on Waves, WMO, Marine Meteorological of Related Oceanographic Activities Report No. 12, 125-138.

No. 36. Burroughs, L.D., 1991: Forecast Guidance for Santa Ana conditions. Technical Procedures Bulletin No. 391, 11pp.

No. 37. Burroughs, L. D., 1989: Ocean Products Center Products Review Summary. Technical Note/NMC Office Note No. 359. 29pp.

No. 38. Feit, D. M., 1989: Compendium of Marine Meteorological and Oceanographic Products of the Ocean Products Center (revision 1). NOAA Technical Memo NWS/NMC 68.

No. 39. Esteva, D. C., Y. Y. Chao, 1991: The NOAA Ocean Wave Model Hindcast for LEWEX. Directional Ocean Wave Spectra, Johns Hopkins University Press, 163-166.

No. 40. Sanchez, B. V., D. B. Rao, S. D. Steenrod, 1987: Tidal Estimation in the Atlantic and Indian Oceans, 3° x 3° Solution. NASA Technical Memorandum 87812, 18pp.

No. 41. Crosby, D.S., L.C. Breaker, and W.H. Gemmill, 1990: A Defintion for Vector Correlation and its Application to Marine Surface Winds. Technical Note/NMC Office Note No. 365, 52pp.

No. 42. Feit, D.M., and W.S. Richardson, 1990: Expert System for Quality Control and Marine Forecasting Guidance. Preprint, 3rd Workshop Operational and Metoerological. CMOS, 6pp.

OPC CONTRIBUTIONS (Cont.)

No. 43. Gerald, V.M., 1990: OPC Unified Marine Database Verification System. Technical Note/NMC Office Note No. 368, 14pp.

No. 44. Wohl, G.M., 1990: Sea Ice Edge Forecast Verification System. National Weather Association Digest, (submitted)

No. 45. Feit, D.M., and J.A. Alpert, 1990: An Operational Marine Fog Prediction Model. NMC Office Note No. 371, 18pp.

No. 46. Yu, T. W. , and R. L. Teboulle, 1991: Recent Assimilation and Forecast Experiments at the National Meteorological Center Using SEASAT-A Scatterometer Winds. Technical Note/NMC Office Note No. 383, 45pp.

No. 47. Chao, Y.Y., 1990: On the Specification of Wind Speed Near the Sea Surface. Marine Forecaster Training Manual, (submitted)

No. 48. Breaker, L.C., L.D. Burroughs, T.B. Stanley, and W.B. Campbell, 1992: Estimating Surface Currents in the Slope Water Region Between 37 and 41°N Using Satellite Feature Tracking. Technical Note, 47pp.

No. 49. Chao, Y.Y., 1990: The Gulf of Mexico Spectral Wave Forecast Model and Products. Technical Procedures Bulletin No. 381, 3pp.

No. 50. Chen, H.S., 1990: Wave Calculation Using WAM Model and NMC Wind. Preprint, 8th ASCE Engineering Mechanical Conference, 1, 368-372.

No. 51. Chao, Y.Y., 1990: On the Transformation of Wave Spectra by Current and Bathymetry. Preprint, 8th ASCE Engineering Mechnical Conference, 1, 333-337.

No. 52. NOT PUBLISHED

No. 53. Rao, D.B., 1991: Dynamical and Statistical Prediction of Marine Guidance Products. Proceedings, IEEE Conference Oceans 91, 3, 1177-1180.

No. 54. Gemmill, W.H., 1991: High-Resolution Regional Ocean Surface Wind Fields. Proceedings, AMS 9th Conference on Numerical Weather Prediction, Denver, CO, Oct. 14-18, 1991, 190-191.

No. 55. Yu, T.W., and D. Deaven, 1991: Use of SSM/I Wind Speed Data in NMC's GDAS. Proceedings, AMS 9th Conference on Numerical Weather Prediction, Denver, CO, Oct. 14-18, 1991, 416-417.

No. 56. Burroughs, L.D., and J.A. Alpert, 1993: Numerical Fog and Visiability Guidance in Coastal Regions. Technical Procedures Bulletin. No. 398, 6pp.

No. 57. Chen, H.S., 1992: Taylor-Gelerkin Method for Wind Wave Propagation. ASCE 9th Conf. Eng. Mech. (in press)

No. 58. Breaker, L.C., and W.H. Gemmill, and D.S. Crosby, 1992: A Technique for Vector Correlation and its Application to Marine Surface Winds. AMS 12th Conference on Probability and Statistics in the Atmospheric Sciences, Toronto, Ontario, Canada, June 22-26, 1992.

No. 59. Yan, X.-H. and Breaker, L.C., 1993: Surface Circulation Estimation Using Image Processing and Computer Vision Methods Applied to Sequential Satellite Imagery. Photogrammetric Engineering and Remote Sensing, 59, 407-413.

No. 60. Wohl, G., 1992: Operational Demonstration of ERS-1 SAR Imagery at the Joint Ice Center. Proceeding of the MTS 92 - Global Ocean Partnership, Washington, DC, Oct. 19-21, 1992.

No. 61. Waters, M.P., Caruso, W.H. Gemmill, W.S. Richardson, and W.G. Pichel, 1992: An Interactive Information and Processing System for the Real-Time Quality Control of Marine Meteorological Oceanographic Data. Pre-print 9th International Conference on Interactive Information and Processing System for Meteorology, Oceanography and Hydrology, Anaheim, CA, Jan. 17-22, 1993.

No. 62. Breaker, L.C., and V. Krasnopolsky, 1994: The Problem of AVHRR Image Navigation Revisited. Int. Journal of Remote Sensing, 15, 979-1008.

No. 63. Crosby, D.S., L.C. Breaker, and W.H. Gemmill, 1993: A Proposed Definition for Vector Correlation in Geophysics: Theory and Application and Oceanic Technology. 10, 355-367.

No. 64. Grumbine, R., 1993: The Thermodynamic Predictability of Sea Ice. Journal of Glaciology, (in press).

No. 65. Chen, H.S., 1993: Global Wave Prediction Using the WAM Model and NMC Winds. 1993 International Conference on Hydro Science and Engineering, Washington, DC, June 7 - 11, 1993. (submitted)

No. 66. Krasnopolsky, V., and L.C. Breaker, 1993: Multi-Lag Predictions for Time Series Generated by a Complex Physical System using a Neural Network Approach. Journal of Physics A; Mathematical and General, (submitted).

No. 67. Breaker, L.C., and Alan Bratkovich, 1993: Coastal-Ocean Processes and their Influence on the Oil Spilled off San Francisco by the M/V Puerto Rican. Marine Environmental Research, 36, 153-184.

No. 68. Breaker, L.C., L.D. Burroughs, J.F. Culp, N.L. Gunasso, R. Teboulle, and C.R. Wong, 1993: Surface and Near-Surface Marine Observations During Hurricane Andrew. Technical Notes/NMC Office Note #398, 41pp.

No. 69. Burroughs, L.D., and R. Nichols, 1993: The National Marine Verification Program - Concepts and Data Management, Technical Note/NMC Office Note #393, 21pp.

No. 70. Gemmill, W.H., and R. Teboulle, 1993: The Operational Use of SSM/I Wind Speed Data over Oceans. Pre-print 13th Conference on Weather Analyses and Forecasting, AMS Vienna, VA., August 2-6, 1993, 237-238.

No. 71. Yu, T.-W., J.C. Derber, and R.N. Hoffman, 1993: Use of ERS-1 Scatterometer Backscattered Measurements in Atmospheric Analyses. Pre-print 13th Conference on Weather Analyses and Forecasting, AMS, Vienna, VA., August 2-6, 1993, 294-297.

No. 72. Chalikov, D. and Y. Liberman, 1993: Director Modeling of Nonlinear Waves Dynamics. J. Physical, (submitted).

No. 73. Woiceshyn, P., T.W. Yu, W.H. Gemmill, 1993: Use of ERS-1 Scatterometer Data to Derive Ocean Surface Winds at NMC. Pre-print 13th Conference on Weather Analyses and Forecasting, AMS, Vienna, VA, August 2-6, 1993, 239-240.

No. 74. Grumbine, R.W., 1993: Sea Ice Prediction Physics. Technical Note/NMC Office Note #396, 44pp.

No. 75. Chalikov, D., 1993: The Parameterization of the Wave Boundary Layer. Journal of Physical Oceanography, (to be submitted).

No. 76. Tolman, H.L., 1993: Modeling Bottom Friction in Wind-Wave Models. Ocean Wave Measurement and Analysis, O.T. Magoon and J.M. Hemsley Eds., ASCE, 769-783.

No. 77. Breaker, L., W. Broenkow, 1994: The Circulation of Monterey Bay and Related Processes. Oceanography and Marine Biology: An Annual Review, 32, 1-64.

No. 78. Chalikov, D., D. Esteva, M. Iredell and P. Long, 1993: Dynamic Coupling between the NMC Global Atmosphere and Spectral Wave Models. Technical Note/NMC Office Note #395, 62pp.

No. 79. Burroughs, L.D., 1993: National Marine Verification Program - Verification Statistics - Verification Statistics, Technical Note/NMC Office Note #400, 49 pp.

No. 80. Shashy, A.R., H.G. McRandal, J. Kinnard, and W.S. Richardson, 1993: Marine Forecast Guidance from an Interactive Processing System. 74th AMS Annual Meeting, January 23 - 28, 1994.

No. 81. Chao, Y.Y., 1993: The Time Dependent Ray Method for Calculation of Wave Transformation on Water of Varying Depth and Current. Wave 93 ASCE.

No. 82. Tolman, H.L., 1994: Wind-Waves and Moveable-Bed Bottom Friction. Journal of Physical Oceanography, 24, 994-1009.

No. 83. Grumbine, R.W., 1993: Notes and Correspondence A Sea Ice Albedo Experiment with the NMC Meduim Range Forecast Model. Weather and Forecasting, (submitted).

No. 84. Chao, Y.Y., 1993: The Gulf of Alaska Regional Wave Model. Technical Procedure Bulletin.

No. 85. Chao, Y.Y., 1993: Implementation and Evaluation of the Gulf of Alaska Regional Wave Model. OPC Office Note, 35 pp.

No. 86. WAS NOT PUBLISHED.

No. 87. Burroughs, L., 1994: Portfolio of Marine Meteorological and Oceanographic Products of the Ocean Products Center (OPC). NOAA Tech Memo. In preparation.

No. 88. Tolman, H.L., D. Chalikov, 1994: Development of a Wind Generation Ocean Wave Model at NOAA/NMC. Proc. Waves Physical and Numberial Modelling University of British Columbia, Vancover. (in press).

No. 89. Peters, C., W. Gemmill, V. Gerald, and P. Woiceshyn, 1994: Evaluation of Empirical Transfer Functions for ERS-1 Scatterometer Data at NMC. 7th Conference on Satellite Meteorology and Oceanography, June 6-10, 1994, Monterey, CA., pg. 550-552.

No. 90. Breaker, L.C., and C.R.N. Rao, 1994: The Effects of Aerosols from the Mt. Pinatubo and Mt. Hudson Volcanio Eruption on Satellite-Derived Sea Surface Temperatures. Journal of Geophysical Research. (To be submitted).

No. 91. Yu, W., P. Woiceshyn, W. Gemmill, and C. Peters, 1994: Analysis & Forecast Experiments at NMC Using ERS-1 Scatterometer Wind Measurements. 7th Conference on Satellite Meteorology and Oceanography, June 6-10, 1994, Monterey, CA., pg. 600-601.

No. 92. Chen, H.S., 1994: Ocean Surface Waves. Technical Procedures Bulletin.

No. 93. Breaker, L.C., V. Krasnopolsky, D.B. Rao, X.-H. Yan, 1994: The Feasibility of Estimating Ocean Surface Currents on an Operational Basis using Satellite Feature Tracking Methods. Bulletin of the American Meteorolgical Society. (In press).

No. 94. Krasnopolsky, L. Breaker, and W. Gemmill, 1994: Development of Single "All-Weather" Neural Network Algorithms for Estimating Ocean Surface Winds from the Special Sensor Microwave Imager. NMC, OPC Contribution Note.

No. 95. Breaker, L.C., D.S. Crosby and W.H. Gemmill, 1994: The application of a New Definition for Vector Correlation to Problems in Oceanography and Meteorology. Journal of Applied Meteolorology. (in press).

No. 96. Breaker, L.C., L.D. Burroughs, Y.Y. Chao, J.F. Culp, N.L. Gunasso, R. Teboulle, and C.R. Wong, 1994: Surface and Near-Surface Marine Observations During Hurricane Andrew. Weather and Forecasting, 9, (in press).


DEPARTMENT OF COMMERCE
UNITED STATES OF AMERICA